J Mater Sci (2021) 56:15513–15537

Review

Stability of ultra-fine and nano-grains after severe plastic deformation: a critical review

Farzad Khodabakhshi[1,2,*], Mohsen Mohammadi[2], and Adrian P. Gerlich[3]

[1] School of Metallurgy and Materials Engineering, College of Engineering, University of Tehran, P.O. Box, 11155-4563 Tehran, Iran
[2] Marine Additive Manufacturing Centre of Excellence (MAMCE), University of New Brunswick, 3 Bailey Drive, P.O. Box 4400, Fredericton, NB E3B 5A1, Canada
[3] Department of Mechanical and Mechatronics Engineering, University of Waterloo, Waterloo, ON, Canada

Received: 21 March 2021
Accepted: 17 June 2021
Published online: 24 June 2021

ABSTRACT

In this critical note, the thermal stability behavior of ultra-fine grained (UFG) and nano-structured (NS) metals and alloys produced through severe plastic deformation (SPD) techniques is reviewed. For this case, the common engineering metals with body-centered cubic (BCC), face-centered cubic (FCC), and hexagonal close-packed (HCP) crystal structures such as aluminum, copper, nickel, magnesium, steel, titanium, and their relating alloys were assessed. Microstructural evolution in these severely deformed materials following post-processing annealing treatment was investigated for various times and temperatures below the recrystallization point. The microstructure development reported in the literature was studied in terms of the stable grain structures correlated with different levels of plastic straining. The stacking fault energy (SFE) is noted to be a key issue which has a critical influence in predicting the coalescence or coarsening behavior of ultra-fine and nanoscale grains after SPD treatment by controlling the cross-slip phenomenon for screw dislocations.

Handling Editor: P. Nash.

Address correspondence to E-mail: fkhodabakhshi@ut.ac.ir; farzadkhodabakhshi83@gmail.com

https://doi.org/10.1007/s10853-021-06274-6

GRAPHICAL ABSTRACT

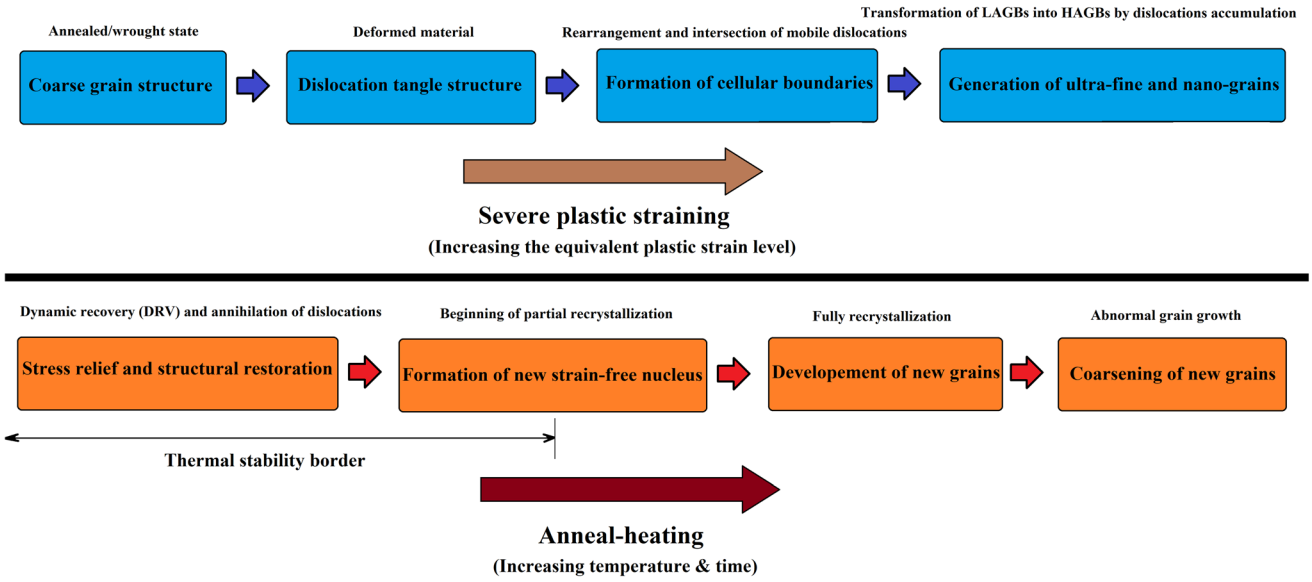

Introduction

In the last decade, the application of lightweight components in hybrid passenger vehicles to reduce weight and corresponding CO_2 emission gains has gained significant attention and motivated the development of advanced metals and alloys [1]. One practical approach to enhance the strength-to-weight ratio for structural materials is refining their grain structure to enhance yield strength through the Hall–Petch mechanism and bolster the consequent strain hardening [2]. Based on the dimensions of a crystalline microstructure, materials can be classified into three categories as; (*i*) coarse-grained (CG) structures with an average grain size of higher than 1 μm, (*ii*) ultra-fine grained (UFG) structures with a mean size in the range of 100 to 1000 nm, and (*iii*) nano-structures (NS) materials with an average length of less than 100 nm [2, 3]. According to the well-established Hall–Petch relation [4], refining the grain structure of materials into the UFG and NS ranges can lead to significant grain boundary strengthening. These classes of materials with superior mechanical properties can be processed through two distinct routes based on "bottom-up" or "top-down" strategies [3, 5].

The principle for bottom-up synthesis is based on the layer-by-layer stacking and consolidation of individual atoms, using high-precision technologies consisting of physical vapor deposition (PVD) and chemical vapor deposition (CVD) methods [3]. For the second methodology, melt spinning (MS), severe plastic deformation (SPD), and electrodeposition are well-developed top-down concepts for producing UFG/NSM materials. By applying rapid cooling followed by SPD through severe plastic shear straining, the grain structure can be refined into the UFG nanoscale ranges without any change in the cross-sectional dimensions of the processed materials [3, 6]. In this context, several SPD techniques have been introduced and implemented for the production of UFG/NS materials based on imposing high strains, such as equal channel angular pressing (ECAP) [3, 6], high-pressure torsion (HPT) [7, 8], accumulative roll bonding (ARB) [9], mechanical alloying (MA) [5, 10–12], multi-axial forging (MAF) [13], cumulative hydrostatic extrusion followed by rotary swaging (HE-RS) [14], constrained groove pressing (CGP) [15, 16], friction stir processing (FSP) [17, 18], and accumulative fold-forging (AFF) [19, 20]. All of these SPD processes have been applied to various kinds of metals and alloys, and the major finding results

highlighted the consistent correlation between microstructural refinement and improved mechanical properties.

Recent attempts to fabricate UFG and NS materials by SPD approaches resulted in the generation of various structural features with potential for commercial applications due to their superior physical and mechanical properties [1, 21]. These processed metallic materials offer multi-functional behavior based on their intrinsic characteristics derived from their nanoscale grain size, misorientation angle of grain boundaries, the formation of sub-cells and micro-twins, dominance of preferred orientations or crystallographic textures, along with the contribution of precipitates and dispersoids [22, 23]. For instance, refining the grain structure down to the nanoscale can yield exceptional superplastic behavior with an excellent combination of tensile strength and elongation to failure [24]. Introducing various structural lattice defects throughout the crystalline material during intense plastic straining including high-misorientation nano-grains, dislocations, and twins can improve the strength-to-weight ratio of components for various structural applications [25, 26]. However, the main concern regarding these UFG or NSM materials during service would be their thermal instability during environmental exposure, especially via heating and loading effects.

For long-term applications at elevated temperatures, microstructural defects can degrade the thermal stability of the produced nano-crystalline materials, although they exhibited a positive impact on the mechanical strength at ambient temperatures [1, 23]. The high level of stored strain energy during repetitive high cycle SPD processing can lead to thermal instability in severely deformed structures. A typical trend observed when increasing the imposed equivalent plastic strain level is the apparent activation energy for subsequent thermal softening phenomena is notably decreased, which can exacerbate unstable behavior. The potential thermal instability of the produced UFG/NS materials via SPD treatment is a major issue due to the high density of dislocations and the fraction of other defects can restrict their commercial applications [27, 28]. This is because these defects promote various thermally driven structural restoration phenomena such as dynamic recovery, static recrystallization, grain growth, and precipitation, which all lead to coarsening of the structure and deterioration of the mechanical strength of materials at higher temperatures [22, 24, 29]. Several factors can affect the thermal stability of UFG and NS materials, including the chemical composition of the alloy, melting temperature, and the presence of lattice defects [1, 24].

In the case of chemically pure materials with a low melting point, self-annealing may occur after SPD treatment by static recrystallization and grain growth phenomena at room temperature, attributing to the higher fraction and mobility of boundaries and lattice defects [22, 23]. The possibility for self-annealing phenomenon in SPD-processed materials can deteriorate the long-term structural thermal stability, making this a critical factor in the stability of structures for several years [21, 25]. Therefore, to improve the thermal stability of these materials, subsequent post-processing operations is crucial. By controlling and optimizing processing parameters in terms of strain, strain rate, and testing temperature during SPD, it would be possible to suppress the kinetics of dynamic recovery and recrystallization softening phenomena by restricting the diffusion-involved mechanisms and reducing the mobility of dislocations [30, 31].

In this critical assessment, the key objective is to overview the reported results in the literature regarding the prominent grain structural aspects after SPD processing for different metals and alloys affected by post-annealing treatment. For various purities of the examined materials, the stable grain size was determined upon SPD modification along with subsequent heating below the recrystallization region. Then, the thermal stability behavior of SPD-processed UFG/NS metals and alloys was modeled to establish and discuss a general correlation between the stable grain size after SPD modification and its coarsening during long-term annealing in service, depending on the intrinsic characteristics of materials in terms of chemical composition, crystallographic structure, and stacking fault energy (SFE).

Importance

In one of the pioneering review articles on the field of UFG/NS materials by Vailev et al. [3], the formation of bulk nano-structured metals and alloys using various routes of SPD processing was overviewed. In this first comprehensive review issue regarding the production of UFG/NS materials through SPD, the

basic concepts for the generation of cellular structures in the ultra-fine or nanoscale ranges upon severe plastic straining were discussed. Moreover, the capability of different SPD routes for achieving the smallest grain size limit in various classes of materials was compared. In the following comprehensive literature survey by Vailev et al. [6], ECAP was specifically attracted significant focus as an alternative route of SPD treatment for grain refinement of metals and alloys. Then, an interesting extensive review has been published by Zhilyaev et al. [32] evaluating the application of HPT methods in terms of principles and performance of products. After that, this review was updated with two short reviews by Edalati et al. [7, 25] on the new achievements. In a recent review by Sakai et al. [33], the high-temperature annealing behavior of cold-worked materials by the occurrence of static and dynamic recrystallization phenomena was studied. The potential of the CGP process for grain structural refinement in the ultra-fine or nanoscale range and mechanical properties improvement of different metals and alloys was assessed in a recent comprehensive review by Gupta et al. [34]. Also, several review articles addressed different prospects of FSP surface modification as an alternative thermo-mechanical route of SPD treatment by applying high strains and strain rates at elevated temperatures [18, 35, 36]. In the review by Kawasaki and Langdon [37], the superplastic behavior of SPD-treated materials with refined grain structures in the range of ultra-fine or nanoscale at high temperatures was studied and discussed. In another reviewing activity by Kumar et al. [38], the strength–ductility trade-off in ultra-fine grained or nano-structured metals and alloys processed by SPD at low temperatures was statistically overviewed and described. More recently, Wang et al. [39] have reviewed the strategies and approaches for improving the low-temperature formability of magnesium and its alloys. However, to the best of the current reviewer's knowledge, there is no review summarizing the literature related to the thermal stability of UFG/NS materials produced by different routes of SPD treatment in connection with their relating mechanical stability. Therefore, the focus of the current critical review article would be on this important object.

Basics for thermal stability of UFG/NS materials

As described before in the literature [3, 6], applying high levels of equivalent plastic strains at low temperatures via various SPD routes can drastically increase the density of statically stored and geometrically necessary dislocations. At first, during primary SPD passes caused by low strain levels, the structure of these dislocations is in the form of a tangle. However, by continuously repeating the SPD process and increasing the strain level, dislocations can interact and rearrange to form cellular structures in ultra-fine or nanoscale ranges. In the following, more generations of dislocations via further straining can increase the density of dislocations through the cellular walls. This can increase the misorientation angle between the cells by gliding dislocations from the cells inside toward the relating walls and accordingly shifts these cellular structures from low-angle grain boundaries (LAGBs) toward more high-angle grain boundaries (HAGBs) [33]. Also, the size of these cells can be reduced via straining; however, the occurrence of dynamic recovery (DRV) can restrict the lowest limit for that. Exposing such ultra-fine grained or nano-structured materials to post-annealing modification would be critical to restoring the severely deformed structure, depending on the processing parameters, since the high density of dislocations within one or two orders of magnitudes more elevated than the annealed state [33]. High-temperature annealing of these SPD-processed structures will experience recrystallization and growth of new grains, diminishing the previous cold work history. Meanwhile, by low-temperature annealing near the recrystallization limit, these UFG/NS materials can display a form of thermal stability behavior depending on their relating chemistry and SFE level. Controlling the restoration mechanisms in DRV and partial recrystallization during this post-annealing modification can preserve the cellular structures within the ultra-fine or nanoscale ranges and stabilize the grain boundaries. However, working close to the thermal stability window is essential. Sometimes, the partial occurrence of non-favorable restoration phenomena in the form of partial recrystallization and grain growth may be unavoidable. In this case, the structural restorations for the severely plastic deformed structures before and after post-

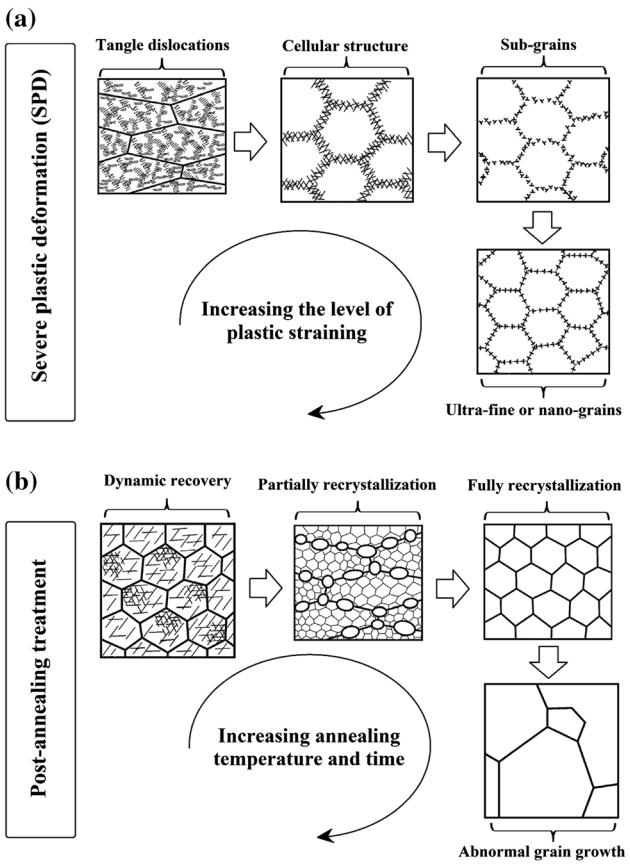

Figure 1 Schematic plots illustrating the mechanisms for grain structural modification during **a** SPD treatment and **b** after post-annealing modification [33].

annealing treatment are schematically demonstrated in Fig. 1a and b, respectively.

Aluminum and its alloys

The main microstructural details for aluminum and its alloys processed by different SPD routes along with a comparison to the as-received condition of these materials have been reviewed in the literature in terms of average grain size before and after post-annealing treatment, and they are summarized in Table 1. The minimum achievable grain size via SPD modification is strongly dependent on the alloy chemistry along with the straining route [40–43]. As reported in the literature [28, 44], the SFE level and solute strengthening can strongly contribute to the formation of ultra-fine or nano-grains during SPD treatment. Consequently, a balance between the generation rate of geometrically necessary dislocations via strain mismatching and their annihilation by the simultaneous operation of dynamic restoration phenomena such as dynamic recovery can be established, and these depend on the alloy chemistry and testing temperature [37, 45, 46]. In this context, a broad range between 100 nm to 1.6 μm has been observed for the mean grain size after SPD, as reported in Table 1 [47–49].

Table 1 The average grain size (D) as treated by different SPD routes before and after intense plastic straining for aluminum and its alloys along with the post-annealing modification

Alloy	Primary state	SPD		Annealing condition		After post-annealing	Refs
	D	Route	D	Temperature	Time	D	
AA1070	36.5 μm	Cryo-rolling	~ 790 nm	473 K	30 min	~ 1 μm	[52]
AA5083	42.2 μm	Cryo-rolling	~ 160 nm	523 K	30 min	~ 760 nm	[52]
AA2014	38.4 μm	Cryo-rolling	~ 100 nm	623 K	30 min	~ 570 nm	[52]
AA1050	35.3 μm	ARB	~ 780 nm	473 K	2 h	~ 1.02 μm	[61]
AA1050	35.3 μm	ECAP	~ 1.01 μm	473 K	2 h	~ 1.49 μm	[61]
Al-Li	–	ECAP	~ 1.6 μm	423 K	1 h	~ 1.1 μm	[62]
AA2024	–	ECAP	~ 250 nm	573 K	1 h	~ 450 nm	[63]
Al-1.6Li	~ 300 μm	ECAP	~ 370 nm	556 K	10 min	~ 730 nm	[64]
AA1100	~ 30 μm	ECAP	~ 700 nm	573 K	1 h	~ 1.5 μm	[58]
AA2024	~ 40 μm	ECAP	~ 200–300 nm	573 K	1 h	~ 600 nm	[58]
AA3004	~ 15 μm	ECAP	~ 200–300 nm	573 K	1 h	~ 1.2 μm	[58]
AA5083	~ 30 μm	ECAP	~ 200–300 nm	573 K	1 h	~ 1.3 μm	[58]
AA6061	~ 50 μm	ECAP	~ 200–300 nm	573 K	1 h	~ 1.1–1.2 μm	[58]
AA7075	~ 30 μm	ECAP	~ 200–300 nm	573 K	1 h	~ 400–450 nm	[58]
AA6016	~ 40 μm	ECAP	~ 210 nm	473 K	1 h	~ 460 nm	[65]
Al-4Cu	–	HPT	~ 210 nm	353 K	5 days	~ 390 nm	[66]

The grain size achievable by SPD treatment is continuously refined by shifting from a pure commercial state toward the alloying chemistry and complexity of alloy composition under the same processing conditions (SPD route and processing temperature) [6, 50]. This can be attributed to the impact of precipitation and the related modifications against the breakup of primary grains and the migration of new boundaries upon the straining route by changing the alloying state of aluminum [28, 40, 41, 43, 46, 47, 51]. Moreover, by employing an SPD route with the higher straining capability such as the HPT method while reducing the processing temperature, the smallest achievable grain size is significantly reduced [40, 41, 45, 49]. For example, in the case of specific alloys such as AA2xxx series, implementation of cryo-rolling processing yielded a finer grain size compared to the ECAP route due to the difference in straining conditions, along with decreasing chemical potential for grain boundary migration by applying a submerged cryogenic cooling medium.

However, the stability of these ultra-fine and nano-grains after SPD processing under the effects of heating phenomena varied considerably depending on the testing situations [41, 46, 51]. Indeed, by further refining the grain structure via SPD treatment, the subsequent susceptibility of the produced UFG/NS materials upon heating exposure would be higher, although the severity of this trend is related to the type of grain boundaries present (such as low-angle versus high-angle), along with the corresponding misorientation between the adjacent grains [1, 52–55]. In addition, the contribution of secondary phase precipitates or nanoparticles within the aluminum matrix depends on the designation and chemistry of the aluminum alloy. This directly affects the material thermal stability after intense grain structural refinement by SPD, since these nano-sized secondary phases can suppress coarsening of ultra-fine or nano-grains by hindering along the boundaries [56, 57]. For the SPD-treated microstructures, as mentioned before, the optimized post-annealing conditions to reach a thermally stable state and the resulting steady-state grain size after annealing action are summarized in Table 1. The optimum temperature and time range for post-annealing modification can vary widely depending on the chemistry of the aluminum alloy, and processing routes. In comparing different aluminum alloy series (AA1100, AA2024, AA3004, AA5083, AA6061, AA7075, and AA6016) with similar initial structures, SPD treatment such as ECAP provides intense plastic deformation in the range of 200–300 nm. It is obvious that the precipitation harden-able alloys such as AA2024 and AA7075 can exhibit more thermally stable behavior as revealed with less coarsening of resulting grain structures due to the role of nanoparticles on stabilizing and pinning the boundaries of nano-sized grains [43, 58–60].

Copper

Similar to other UFG/NS metals and alloys, the structure of SPD-processed copper-based materials also deteriorates with environmental heating exposures due to the presence of a cellular structure along with a high density of dislocations [67]. Depending on the applied plastic strain level, the extent and degree of thermal instability can vary. Incrementally increasing the imposed strain during SPD treatment can result in a gradual destabilizing of the severely deformed microstructure [67]. According to the reports, enhancing the level of stored strain energy through the structure as well as reducing the testing temperature upon SPD processing can improve the mobility of atoms in the presence of material defects [31, 68]. In general, by increasing the SFE, the average grain size after SPD treatment can increase due to the activation of the cross-slip mechanism to mobilize screw dislocations according to combining the partial dislocations [69].

In the case of copper-based alloys, the solid-solution strengthening is a key mechanism to predict the saturation state for the grain size after SPD modification as reported in the literature [31, 68, 70–73]. This saturation limit is primarily determined by the melting temperature of the material, where the value of the SFE does not play a significant role, especially for SPD treatment at room temperature. Also, the role of twinning deformation can be intensified by increasing the SFE level. Introducing a dense network of twin boundaries by SPD straining of copper can stabilize the microstructure with a higher recrystallization temperature than the nano-structured materials, including the cellular and equiaxed grains [67]. The condition for thermal stability can be expressed as the temperature for the beginning of recrystallization before abnormal grain growth. For the pure

Table 2 The average grain size (D) for copper-based alloys after SPD and post-annealing treatments

Alloy	Primary state	SPD		Annealing condition		After post-annealing	Refs
	D	Route	D	Temperature	Time	D	
Cu	–	HPT	~ 84 nm	523 K	1 h	~ 650 nm	[69, 82]
Cu-10Zn	–	HPT	~ 54 nm	–	–	–	[69]
Cu-30Zn	–	HPT	~ 17 nm	–	–	–	[69]
Cu	–	HPT	~ 107 nm	573 K	1 h	~ 1.3–1.4 μm	[76]
Cu-0.5wt% Al2O3	–	HPT	~ 80 nm	1073 K	1 h	~ 2.5 μm	[78]
Cu	–	ECAP	~ 45 nm	453 K	40 min	~ 290 nm	[83]
Cu	~ 60 μm	ECAP	~ 200 nm	473 K	30 min	~ 5 μm	[84]
Cu-Cr-Zr	~ 120–150 μm	ECAP	~ 400 nm	773 K	1 h	~ 800 nm	[85]
Cu-Nb	~ 40–80 μm	HPT	~ 100–200 nm	773 K	1 h	~ 400–500 nm	[74]
Cu-Co	–	HPT	~ 90 nm	873 K	100 h	~ 410 nm	[80]
Cu-Ta	–	HPT	~ 10 nm	1273 K	1 h	~ 200–500 nm	[77]
Cu-Be	–	HPT	~ 20 nm	548 K	10 h	~ 70 nm	[86]
Cu–Zn	50 μm	CGP	~ 20–25 μm	573 K	10 min	~ 20–25 μm	[87]
Cu	–	HPT	~ 100 nm	873 K	1 h	~ 265 nm	[81]

state of the alloy, both the melting temperature and SFE level are key controlling parameters to determine the final microstructure after annealing the SPD-processed structure. In copper-based alloys, the rate of grain growth during annealing modification could be oppositely related to the solid-solution influence [69].

Based on the reported microstructural investigations in the literature, the interaction of dislocations according to the glide and kink nucleation mechanisms is the main phenomenon controlling the thermal stability of copper based UFG/NS fabricated by SPD below the recrystallization temperature [74]. However, at higher temperatures, the plastic deformation behavior can be controlled by the role of thermally activated phenomena depending on the testing temperature as well as the strain and strain rate magnitudes applied [74]. Rapid diffusion and enhanced transformation kinetics along the large fraction of grain boundaries can make the structure less stable with a high susceptibility to coarsening, deteriorating the microstructure and subsequent induced mechanical properties [75]. Examinations revealed the significance of structural relaxation beside the typical grain growth in predicting the thermal stability of ultra-fine grain boundaries [76]. Considering the reported data in Table 2 summarizing the microstructural details of SPD-processed materials by various SPD techniques followed by varying post-annealing conditions, the thermal stability temperature with time for the produced UFG structure of commercially pure copper after SPD treatment is close to 448 K up with a 1 h holding time. However, the addition of alloying elements or second-phase particles has a strong effect on the thermal behavior of the resulting UFG/NS materials (see Table 2). For instance, by alloying the copper matrix with tantalum, it was possible to achieve an average size of ~ 10 nm via HPT without abnormal coarsening when annealing at 1273 K for 1 h [77]. Following this annealing, the mean grain size coarsened to the range of 200 to 500 nm. The incorporation of 0.5 *wt*% Al_2O_3 nanoparticles in the structure further enhances pinning of the ultra-fine grain boundaries improving the thermal stability to allow an annealing at 673 K for one hour with a similar final grain size [78].

In general, structural stabilization of the UFG/NS materials after treatment by SPD processing often involves three different strategies as follows: (i) thermal annealing below the recrystallization region, (ii) changing the slip character from wavy path to other ones, and reinforcing/pinning of the grain boundaries by (iii) solid-state precipitates and (iv) particle agents [79]. Considering the kinetic and thermodynamic aspects, dispersing solute elements along grain boundaries as well as the segregation or re-dissolution of secondary phase precipitates at the junctions' during annealing can be highly effective stabilizing the ultra-fine or nanoscale interfaces [80]. An exciting

Table 3 The average grain size (D) for nickel and nickel-based alloys as treated by different SPD routes before and after intense plastic straining along with the post-annealing modification

Alloy	Primary state	SPD		Annealing condition		After post-annealing	Refs
	D	Route	D	Temperature	Time	D	
Ni	–	HPT	~ 115 nm	473 K	1 h	~ 250 nm	[76, 82]
Ni	~ 30 μm	ECAP	~ 350 nm	523 K	3600 s	~ 950 nm	[88]
Inconel 718	~ 40 μm	MAF	~ 20–50 nm	973 K	5 min	~ 300 to 500 nm	[13]
Ni-20%Cu	~ 80 μm	MAF	~ 50 nm	873 K	30 min	~ 100 to 300 nm	[13]
Ni	~ 200 μm	ECAP	~ 200 nm	673 K	1 h	~ 1 μm	[93]
Ni	–	CGP	~ 17 μm	873 K	1 h	~ 22 μm	[94]
Ni-0.5wt% CNT	~ 20 μm	HPT	~ 50 nm	773 K	1 h	~ 200 nm	[91, 92]

report by Qi et al. [81] revealed that the contribution of pores within the microstructure of severely deformed materials can also introduce drag agents to impede the migration of grain boundaries and accordingly stabilize the structure after heat treatment. Based on this report, the nano-structure of commercially pure copper after HPT processing can exhibit a stable thermal behavior up to the temperature of 873 K, as reported in the last row of Table 2.

Nickel

Considering the great formability combined with an elevated melting point and high stacking fault energy, nickel and its alloys are excellent materials for processing via SPD routes to create ultra-fine or nano-sized grain structures. Similar to other FCC metals and alloys such as aluminum and copper-based materials, nickel can exhibit superior plastic deformation capacity due to the presence of 12 independent easy slip systems. According to experimental investigations [76, 82], the thermal stability behavior of ultra-fine grained or nano-structured commercial pure nickel processed via SPD treatment can be controlled by various factors in terms of average grain size as well as the contribution of statistical and geometrically necessary dislocations along the boundaries. Based on the results, the density and distribution of dislocations across the grain boundaries can be relaxed upon post-annealing treatment at around 448 K to increase structural thermal stability [82]. As summarized in Table 3, the severity of grain structural refinement for nickel and its alloys depends on the route of SPD processing as well as the chemistry of the examined alloy. In this case, the minimum achievable grain size after SPD treatment of commercially pure nickel is different for ECAP, HPT, and CGP routes, which was reported as 200 nm, 115 nm and, 17 μm, respectively. In the case of SPD-processed material the stability behavior of the fabricated UFG or NS materials depends on the thermal modification to control the recovery, recrystallization, and coarsening phenomena, which are strongly correlated with the composition and chemistry of the alloys. As described in the literature, the kinetics for growth of ultra-fine grained or nano-structured nickel after SPD treatment are controlled by the grain boundary diffusion due to the contribution of short circuits for diffusion of elements in the deformed structure [88].

According to the experimental results listed in Table 3, compared to the other FCC metals and alloys such as aluminum and copper-based materials, nickel can exhibit a moderate thermal stability behavior imparted by a higher melting temperature along with the range of SFE level. Although, for the nickel alloys and nickel-based nano-composites, this scenario would be drastically changed due to the role of precipitates and nanoparticles in stabilizing and pinning the material structure in the ultra-fine or nanoscale range. In fact, by adding alloying elements and precipitating complex compounds in the nickel matrix, the thermal stability of the nickel-based nano-structures after severe plastic deformation can be improved [89]. In the case of these nickel-based alloys, the type and size distribution of fine second-phase particles or precipitates and their interactional bonding with the metal-matrix are the important structural parameters to control the severely deformed materials thermal stability [90]. Regarding

the formation of precipitates, the diffusivity of solute elements within the metal-matrix is a critical factor, although a high diffusivity can lead to the precipitates coarsening through the ultra-fine grained or nano-structure. Similar to other metals and alloys, the thermal stabilization of nano-crystalline nickel-based structures processed by SPD can be predicted according to the various approaches. However, the most effective strategy relates to the kinetic stabilization by pinning the grain boundaries using the Zener-pinning effect [13]. In this case, the role of secondary phase agents in the form of nano-sized particles or precipitates with a specific volume fraction would be hindering the grain boundary migration through classical Zener drag [13]. The uniform dispersion of nanoparticles between the boundaries is a critical parameter for controlling the coalescence rate of nano-grains, thus increasing the annealing temperature [91, 92]. These stabilized nano-structures in the class of precipitation-treatable alloys exhibit excellent potential to delay the coarsening during annealing and open the new windows to extend the utility of these materials in new applications.

Steels

Multiple reports have involved grain structure modification of ferrite by SPD treatment at room temperature and noted the simultaneous activation of multi-slip systems and mechanical fragmentation was a significant factor in microstructure development. Thin shear bands can be formed which align with dislocation cell boundaries at early stages of straining [95]. Then, by activating new slip systems, the parallel band boundaries generated in the previous step can become more serrated [96]. The microstructural refinement can tend toward forming a homogenous ultra-fine grained structure with an equiaxed morphology by continuing this straining process. It is worth recognizing that during plastic deformation of BCC structures such as steel-based materials, $< 111 > \{110\}$, $< 111 > \{112\}$, and $< 111 > \{123\}$ are three typical operative slip systems [97, 98].

The lack of enough active slip systems, since at least five independent ones are necessary during uniaxial loading, along with the presence of pearlitic cementite phase can lead to brittle deformation behavior in steels. Therefore, in the case of medium- or high-carbon steels treated by various SPD routes, the contribution of hydrostatic pressure is very critical to control the principal deformation mode, since pure shear or shear associated with the deformation rotation can lead to activation of extra slip systems [99]. In general, two types of fragmented structures and transitions, including cellular and fragmented boundaries, were determined after SPD processing of carbon steel materials depending on the straining level and the state of internal stresses. In fact, by continuing the straining path, the transition state can be completed by continuing the grain structure evolution from fragmented toward cellular [100]. Considering the expressed experimental data in Table 4 regarding the grain structural refinement after SPD treatment, one finds that the smallest achievable grain size broadly varies from the range of 10 to

Table 4 The average grain size (D) for different grades of steels as treated by different SPD routes before and after intense plastic straining along with the post-annealing modification

Alloy	Primary state	SPD		Annealing condition		After post-annealing	Refs
	D	Route	D	Temperature	Time	D	
Low-carbon steel	~ 30 μm	ECAP	~ 200–300 nm	813 K	1 h	~ 500–600 nm	[99]
Low-carbon steel	–	ECAP	~ 200 nm	753 K	72 h	~ 500 nm	[103]
Iron	–	HPT	~ 100 nm	773 K	1 h	~ 300 nm	[100]
316 austenitic stainless steel	~ 40 μm	HPT	~ 40 nm	1073 K	10 min	~ 380 nm	[29]
304 austenitic stainless steel	~ 40 μm	HPT	~ 300–400 nm	673 K	1 h	~ 1 μm	[29]
Low-carbon steel	~ 30 μm	CGP	~ 230 nm	673 K	20 min	> 1 μm	[15, 27, 101, 106]
Carbon steel (UIC 860 V)	–	HPT	~ 10 nm	873 K	1 h	~ 740 nm	[107]
Ferritic/martensitic steel (T91)	~ 10 μm	ECAP	~ 300–400 nm	973 K	1 h	~ 500 nm	[105]

400 nm, depending mainly on the chemistry of the steel as well as the SPD route.

However, the synergic role of stored strain energy caused by SPD treatment and structural restoration at high temperature during annealing modification can lead to the formation of cellular and fragmented structures with an average size as fine as 300 nm up to the micron-scale, while comprising mostly high-angle grain boundaries [100]. Table 4 summarizes these results for the annealing treatment of SPD-modified steels. As shown, the thermal stability conditions (temperature and time) considerably vary by changing the steel composition and the straining state. According to the studies by Khodabakhshi et al. [27, 101] on the thermal stability behavior of ultra-fine grained low-carbon steel sheet processed by the CGP route of SPD modification, the ultra-fine grains exhibit stable behavior by post-annealing treatment up to a critical temperature of 673 K. Meanwhile, annealing at higher temperatures yields abnormal grain growth that occurs in the severely deformed structures. In the case of ultra-fine grained low-carbon steel materials processed by SPD, a post-annealing treatment can be applied to stabilize the deformed sample structure by the generation of elongated grains with aligned dislocations around the boundaries [102]. This signifies the occurrence of dynamic recovery in the dislocation tangle structure, associated with the absorption and trapping of lattice dislocations within the grain boundaries [103]. In order to control the range of grain size distribution following recovery, recrystallization, and grain coarsening, the annealing conditions, purity, and the state of internal stresses/strains are the crucial factors [104].

According to experimental investigations, intense plastic straining can lead to carbon dissolution from the cementite phase through the ferrite grains of the matrix to stabilize the boundaries upon annealing treatment based on the activation of the solute-drag mechanism. However, by increasing the temperature of post-annealing treatment to above the recrystallization temperature, the pearlite colonies can act as the heterogeneous nucleation sites for full recrystallization of the ferritic grain structure. In the presence of some alloying elements such as vanadium, there is a possible scenario to change the morphology of the pearlitic cementite phase from lamellar plates to particulate shapes upon post-annealing, thus increasing the recrystallization temperature by shifting the microstructure of the deformed material toward a non-equilibrium state [105]. As a result, for this kind of modified steel containing vanadium, a high density of dislocations is formed compared to carbon steels, along with non-equilibrium grain boundaries, which provide preferred paths for diffusion of carbon from the pearlite colonies into the ferritic matrix. The chance of long-path distribution of dissolved carbon is also restricted due to limited easy-diffusion paths and hindering cementite nanoparticles formed around pearlite colonies. However, due to long-range diffusion of carbon in vanadium-modified steels, precipitation of nano-sized cementite particles along the ferritic grain boundaries during annealing treatment can retard the rate of grain boundary migration and coalescence in the next steps of annealing.

In the case of austenitic stainless steels such as 316 and 304 grades, the thermal stability behavior can highly vary depending on the grade of alloy and its related chemistry. For these alloys under the severely plastic deformed state, the transformation of α′-martensite and ε-martensite from the primary austenite phase upon post-annealing treatment is critical to control the microstructure thermal stability. The heterogeneous distribution of ε-martensite within the austenite matrix can be the preferred site for nucleation and transformation to the α′-martensite. The rejection of solute atoms from the martensite phase into the austenite matrix during annealing treatment to form either the new precipitates or segregate along the grain boundaries can improve the thermal stability of the deformed material [29]. As reported in Table 4, the ferritic/martensitic steel of grade T91 exhibits superior thermal stability with a high annealing temperature of up to ~ 973 K after SPD modification by ECAP route. For this alloy, the annealing recovery of the deformed microstructure based on the dislocation annihilation mechanism can be retarded up to a high-temperature range of 923–973 K [105].

Magnesium and its alloys

The use of SPD treatment of magnesium and its alloys has been widely examined in the literature due to the potentially high specific strength that may be achieved as a result of the low density of these metals [39]. However, SPD fabrication at room temperature

Table 5 The average grain size (D) for magnesium-based alloys as treated by different SPD routes before and after intense plastic straining along with the post-annealing modification

Alloy	Primary state	SPD		Annealing condition		After post-annealing	Refs
	D	Route	D	Temperature	Time	D	
AZ31	~ 13 μm	CGP	~ 0.4–1.0 μm	523 K	1 h	~ 5.6 μm	[116]
AZ31	~ 25–30 μm	Rolling	~ 2–3 μm	523 K	1000 min	~ 8.0 μm	[117]
AZ31	~ 25–30 μm	ECAP	~ 7 μm	523 K	1000 min	~ 14 μm	[117]
ZK60	~ 8.5 μm	Rolling	~ 1–2 μm	523 K	24 h	~ 2.8–3.1 μm	[118]
Mg10Gd	~ 10 μm	HPT	< 100 nm	573 K	1 h	~ 100 nm	[30]
AZ31	~ 17 μm	ECAP	~ 500 nm	573 K	30 min	~ 2.6 μm	[119]
AZ61	~ 15 μm	Rolling	~ 1.5 μm	523 K	1 h	~ 2–3 μm	[112]
AZ31	–	ECAP	~ 940 nm	573 K	1 h	~ 2.06 μm	[120]
AZ31	–	ECAP	~ 3.8 μm	623 K	1 h	~ 10 μm	[121]
Mg-8Gd-3Y-0.4Zr	~ 56 μm	HPT	~ 80 nm	623 K	1 h	~ 1.6 μm	[122]

by most routes to large equivalent plastic strains is not possible due to the lack of active independent slip systems in the HCP crystal structure of these materials. In general, magnesium-based metals are classified as difficult materials for cold working, due to the restricted number of slip systems. Therefore, imposing high plastic strains on magnesium alloys via SPD modification is impossible, considering the brittle nature of these materials during large-scale deformation [108]. In this case, the leading microstructural aspect in the form of average grain size for various magnesium alloys after SPD treatment and subsequent post-annealing modification is summarized in Table 5. These data reported for all SPD routes (CGP, ECAP, HPT, and rolling) typically involve applying small strains by the primary passes. According to experimental observations, higher pass numbers or large strains induce fracture in the magnesium part due to severe shear-banding. The occurrence of adiabatic shear-banding for magnesium alloys can be described based on a recrystallization model that increases the misorientation angle between the sub-grains. The mechanism for shear-band formation in magnesium alloys can be explained as follows. Deformation-associated recovery subdivides the equiaxed sub-grains during straining. These equiaxed cells then start to rotate after reaching a critical size by increasing the misorientation angle between sub-grains, leading to banding along the shear direction [109]. Hence, as shown in Table 5, the minimum grain size range attained by SPD of magnesium alloys is considerably larger than in FCC metals and alloys. A typical range of around a micron can be stated for AZ31 and AZ61 magnesium alloys for example. Moreover, the refined grain structure of the HCP alloys after severe cold working is susceptible to deterioration on heating; it exhibits poor thermal stability due to an abnormal rate of grain coalescence. By evaluating the experimental data in Table 5, it seems that the thermal stability temperature for severely plastic deformed magnesium alloys is below 523 K. However, for commercial magnesium alloys such as AZ31, AZ61, and ZK60, even by applying low-temperature annealing treatments, the intense grain growth is significant, resulting in grains with dimensions in the range of several microns [110, 111]. As shown for two alloys' chemical composition, gadolinium is a practical element to modify magnesium's chemistry. In situ formation of precipitates and their distribution along the grain boundaries can reduce the mobility of lattice dislocations and migration of interfaces by exerting a pinning force [112]. Similarly, the contribution of secondary phase thermally stable nanoparticles would result in the Zener-drag pressure and hindering the grain boundary coalescence [113–115]. The volume fraction and size distribution of these secondary phase inclusions are imperative to maximize the pinning force of particles for inhibiting the grain growth and stabilizing the ultra-fine or nanograins after SPD.

Table 6 The average grain size (D) for titanium and titanium-based alloys as treated by different SPD routes before and after intense plastic straining along with the post-annealing modification

Alloy	Primary state	SPD		Annealing condition		After post-annealing	Refs
	D	Route	D	Temperature	Time	D	
CP-Ti grade 2	~ 30 μm	HE-RS	< 90 nm	773 K	1 h	< 500 nm	[14]
CP-Ti grade 2	~ 30–60 μm	ECAP	~ 190 nm	723 K	1 h	~ 200–300 nm	[125]
CP-Ti	–	ECAP	~ 60 nm	850 K	10 min	~ 164 nm	[83]
CP-Ti	~ 10 μm	ECAP	~ 260 nm	673 K	1 h	~ 200–300 nm	[123]
CP-Ti grade 2	~ 10 μm	Rolling	~ 80 nm	673 K	30 min	~ 160 nm	[126]
Ti-45wt% Nb	~ 15 μm	HPT	~ 50 nm	673 K	30 min	~ 200 nm	[124]

Titanium

Titanium and its alloys are ideal metals for biomedical applications and are commonly used for non-biodegradable implants considering their excellent electrochemical properties and inert behavior in situ with human tissue and body fluids. Among the different titanium grades used for structural medical components, commercial pure titanium (CP-Ti) has superior biocompatibility, while its application can be restricted by inferior mechanical strength compared to titanium alloys. Hence, to enhance performance for load-bearing medical implants, modified alloys such as Ti-6Al-4 V are widely employed. However, the addition of alloying elements like aluminum and vanadium can thwart the biocompatibility of the alloy. Therefore, improving the mechanical strength of CP-Ti is a fundamental challenge in biomedical engineering. To this end, SPD is a practical approach to enhance the strength-to-weight ratio of CP-Ti by refining the grain structure of alloy into the ultra-fine or nanoscale range. Accordingly, the Ti-6Al-4 V alloy can be replaced with the modified UFG/NS CP-Ti alloy for medical applications. However, the stability of produced ultra-fine or nano-sized grains after SPD treatment would be a critical parameter during service conditions. By analyzing the reported data regarding the annealing modification of the created UFG/NS structures, shifting the results toward a saturation state of grain stability can be noted. Table 6 illustrates the microstructural evolution for CP-Ti alloys fabricated by different SPD routes (HE-RS, ECAP, rolling, and HPT) and subsequent annealing modifications. As shown, the minimum possible grain size for grade 2 of CP-Ti alloy before annealing can range from 60 to 260 nm, depending on the route of SPD treatment. The low-temperature annealing of the severely deformed CP-Ti alloy below 623 K can yield structural relaxation or recovery by reducing the internal defects via annihilation and rearrangement of dislocations. However, post-annealing at temperatures higher than 723 K can lead to the large-scale recrystallization phenomena. By annealing modification of cold-worked titanium structures, a grain morphology transition can occur from irregular or fibrous cellular structure, toward an equiaxed shape due to a decreasing density of dislocations upon heating [123]. According to published experimental data, it can be stated that the ultra-fine grained CP-Ti alloy is thermally stable up to a critical temperature of 773 K, which is one-hundred degrees higher than the grade 5 of Ti-6Al-4 V alloy [14]. As reported in Table 6, by adding the alloying elements such as niobium, more significant grain structural refinement can be achieved via SPD treatment, and higher thermal stability during subsequent annealing modification can be expressed. This promising behavior is attributed to the simultaneous contribution of α and β phases from the thermodynamic equilibrium derived from the Ti-45*wt*%Nb alloy system at elevated temperatures. In this context, the β-phase is metastable at room temperature that can nucleate by heating to the annealing range. However, the α-phase is thermodynamically stable and has a high chance of formation during severe plastic straining by the intense generation of ultra-fine grains and triple-junctions as the preferred nucleation sites and desired paths, which improve the diffusion of elements [124].

Role of chemical composition and SPD method on long-term thermal stability

The generation of lattice defects throughout the material crystalline structure depends on the stored strain energy level along with the dislocation mobility influenced by the thermal activation phenomena. These issues control the thermal stability of UFG or NS materials based on the occurrence of self-annealing via recrystallization and grain growth mechanisms [69, 127]. In general, the melting temperature is an important parameter to control the thermal stability behavior of processed materials via SPD. By increasing the melting temperature of alloys along with increasing the level of applied equivalent plastic strain, and decreasing testing temperature, the fraction of lattice defects and the level of stored strain energy are significantly increased [128, 129]. However, despite the larger fraction of lattice defects at higher melting temperatures, their mobility through the lattice is lower due to suppression of atomic diffusion, making the structure more stable [130, 131]. Meanwhile, simultaneously increasing the stored energy via straining combined with reducing the processing temperature through activation of the atomic mobility mechanism enhanced by generating lattice defects can promote better thermal instability in the severely deformed structure [33, 130, 131].

Another key factor in controlling the trend of microstructural evolutions is hydrostatic pressure. Although the steady-state density of dislocations and grain boundaries during deformation is independent of applied pressure, the fraction of vacancies can be improved at higher hydrostatic pressures due to suppression of atomic mobility [69, 132, 133]. The processed thermal stability of the material may be deteriorated by the enhanced atomic diffusion, which is proportional to the density of vacancies [130, 132, 134, 135]. In this case, the stacking fault energy (SFE) is a critical factor to control the mobility of the dislocations, and thus the enhanced stored strain energy by the accumulation of dislocations can accelerate the self-annealing phenomenon [69, 127, 129]. Indeed, it has been shown the SFE parameter has a minor influence on the fraction of high-angle grain boundaries [130, 132, 134, 136].

A strong relationship between the SFE value and strain hardening behavior can be inferred based on the control of the cross-slip of screw dislocations to overcome the pinning sites or mobility barriers, and this can induce a wavy to planar slip character transition [129, 131, 132]. In fact, the glide of dislocations can be restricted by reducing the SFE level. The SFE is thus a critical intrinsic structural factor, which will control the extent of DRV during SPD straining and subsequent recrystallization during annealing of severely deformed microstructures [33, 131]. The fundamental driving force behind this disordering is the sequence of crystallographic planes in terms of SFE is structure, which tends toward reducing the

Table 7 The melting temperature and stacking fault energy as reported in the literature for the examined various metals and alloys in this study

Materials	Processing state	Melting temperature (Tm)	Stacking fault energy (SFE)	Refs
	Pure	933.3 K	~ 210 mJ.m-2	[143, 144]
Aluminum alloys	AA1070	926.6 K	~ 166 mJ.m-2	[145, 146]
	AA5083	843 K	~ 33.1 mJ.m-2	[144]
	AA2014	783 K	~ 97.9 mJ.m-2	[147]
	AA5052	880 K	~ 65.3 mJ.m-2	[144]
Copper	Commercial pure	1356 K	~ 80 mJ.m-2	[148]
	Bronze (Cu-10Zn)	1293–1298 K	~ 35 mJ.m-2	[69]
	Brass (Cu-30Zn)	1193–1223 K	~ 14 mJ.m-2	[69]
Nickel	Commercial pure	1981 K	~ 90 mJ.m-2	[145]
Magnesium	Commercial pure	923 K	~ 126 mJ.m-2	[145]
	AZ31, AZ61, AZ91	883 K, 798–883 K, ≥ 694 K	~ 48 mJ.m-2	[149]
Iron	Pure	1811 K	~ 180 mJ.m-2	[147]
Steel	Austenitic stainless	1783 K	< 10 mJ.m-2	[145]
Titanium	Commercial pure	1941 K	~ 15 mJ.m-2	[150]

Gibbs free energy according to a preferred lower energy path [33, 128, 130]. This leads to dislocation dissociation into Shockley partials, thus driving a reduction in total energy. As a result of the expressed interruption, dislocations can divide into two partial components. The induced repulsive and attractive forces between the partial dislocations determines the equilibrium spacing of the partial dislocations, which is equivalent to the stacking fault width [131, 136, 137]. Based on the Cottrell theory [138], the average distance between partial dislocations is under an inverse correlation with the SFE according to the below relationship:

$$d = \frac{G(b_2 b_3)}{2\pi\gamma} \quad (1)$$

where d is the separation distance between partial dislocations, G is the shear modulus for the matrix material, b_2 and b_3 are the Burger's vector for partial dislocations, and γ is the stacking fault energy for the material. A higher SFE level with a lower spread between partial dislocations can make the cross-slip phenomenon for screw dislocations easier, which can lead to faster DRV even when processing temperature is reduced [33, 50, 132, 133, 137]. However, in the case of low and medium levels of SFE, combining the partial dislocation components would be the controlling parameter as this presents an obstacle to cross-slip and rearrangement of dislocations during DRV [130, 131].

The SFE values for typical metals and alloys reported in the literature are summarized in Table 7 for comparison. Commercially pure aluminum has a relatively high SFE of $\sim$ 210 mJ.m^{-2}, which is associated with faster kinetics for spontaneous DRV during straining and the increased tendency for recrystallization after annealing would be favorable. Adding different alloying elements to aluminum, such as Zn, Mn, Si, Mg, and Cu, reduces the SFE value and retard the recovery rate. Magnesium has a particularly effective influence in the case of the AA5xxx aluminum alloy series. This could be due to the active role of solute drag by the action along with the pinning dominancy by the particles on the aluminum matrix [60, 130, 133]. The inherent non-equilibrium state of severely deformed materials due to the contribution of defects such as vacancies and dislocations makes the structure very susceptible to accelerated restoration and abnormal grain growth [33, 136, 139, 140]. However, the presence of secondary phase inclusion in the form of particles and precipitates, especially in the nanoscale range, help to pin the boundaries through Zener effects and hinder the rate of their subsequent coalescence, which shifts the deformed structure toward a higher degree of thermal stability [141, 142].

Calculation of activation energy for annealing growth of severely plastic deformed ultra-fine or nanoscale grains

The following empirical formula can be employed to mathematically predict the kinetics of grain growth during post-annealing treatment of SPD-modified microstructures for various holding times (t) [151]:

$$d^n - d_0^n = kt \quad (2)$$

where $_d$ is the average grain size (before and after annealing treatment), n is the grain coarsening exponent, and k is a factor demonstrating the grain boundary migration. The interface mobility parameter can be expressed according to the well-established classical Arrhenius exponential relationship below, based on the thermal annealing temperature (T) [52]:

$$k = k_0 \exp\left(\frac{Q}{RT}\right) \quad (3)$$

where k_0 is the pre-exponential constant, Q is the activation energy for grain growth and coalescence, and R is the universal gas constant. The following general equation can be derived to predict the kinetics for recrystallization of severely plastic deformed ultra-fine or nano-structures by combining the mentioned equations:

$$d^n - d_0^n = k_0 t \exp\left(-\frac{Q}{RT}\right) \quad (4)$$

Furthermore, the pre-exponential factor of k_0 can be determined fundamentally according to the following expression [88]:

$$k_0 = \frac{4\gamma\Omega}{\delta^2}\left(\frac{\delta D_{0b}}{kT}\right) \quad (5)$$

In the above relation, the parameters of γ, Ω, δ, δD_{0b}, k and T are related to the surface energy of grain boundaries, the atomic volume, the width of grain boundaries, grain boundary diffusion exponential factor, Boltzmann constant, and temperature, respectively [88].

It is worth mentioning that the processing history of the SPD-treated material containing ultra-fine or nano-grains, as well as the dislocation density, can be introduced in defining the pre-exponential factor and activation energy value [28, 40, 47–49]. Accordingly, the coarsening rate of ultra-fine or nano-grains during post-annealing after SPD modification could be entirely different from the rates observed in the as-received or commercial state [52, 68]. Plotting the average grain size square difference versus the inverse of testing temperature based on Eq. (4) can yield the estimation of activation energy for annealing restoration of SPD-treated metals and alloys. This calculation was performed for aluminum and its alloys, commercial pure copper, commercially pure nickel, low-carbon steel, AZ31 magnesium alloy, and commercially pure titanium. The results are illustrated in Figs. 2, 3, 4, 5, 6 and 7, respectively. By considering these trends combined with the experimental results listed in Tables 1, 2, 3, 4, 5 and 6, the mentioned hypothesis regarding the higher temperature sensitivity through further grain structural refinement upon SPD treatment can be supported. Severely deformed microstructures in the lower limiting range of 100 to 200 nm tend to exhibit higher coarsening rates to reach the thermally stable regime with lower activation energy and vice versa. Also, for alloys with a small fraction of precipitates within their structure, lower annealing activation energy compared to the pure states of these metals can display more thermal behavior stability. As a critical

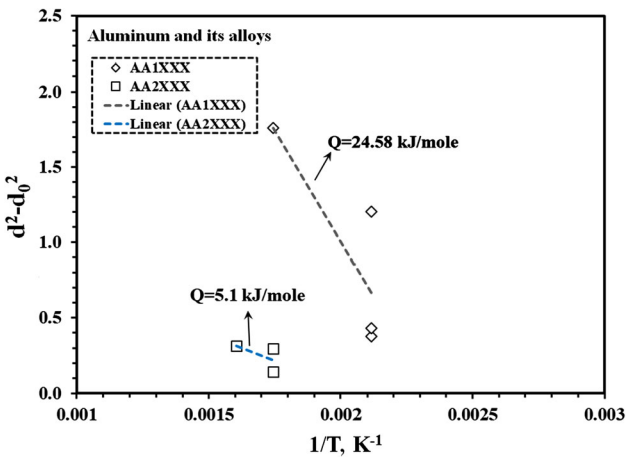

Figure 2 Determination of the activation energy for annealing restoration of SPD-treated aluminum and its alloys by plotting the grain size square difference versus the inverse of testing temperature.

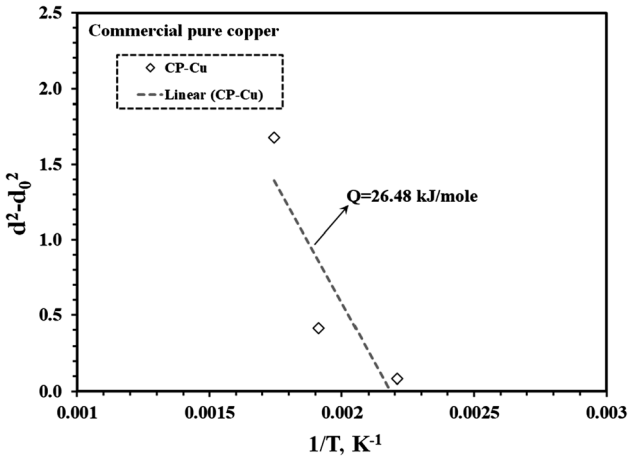

Figure 3 Calculation of activation energy for post-annealing treatment of SPD-modified commercial pure copper.

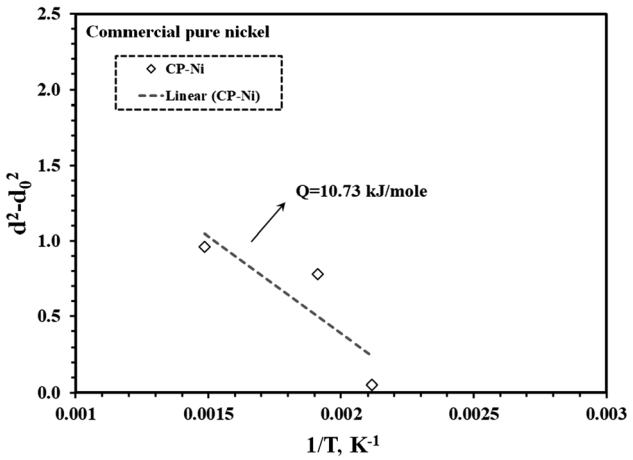

Figure 4 Calculation of activation energy for post-annealing treatment of SPD-modified commercial pure nickel.

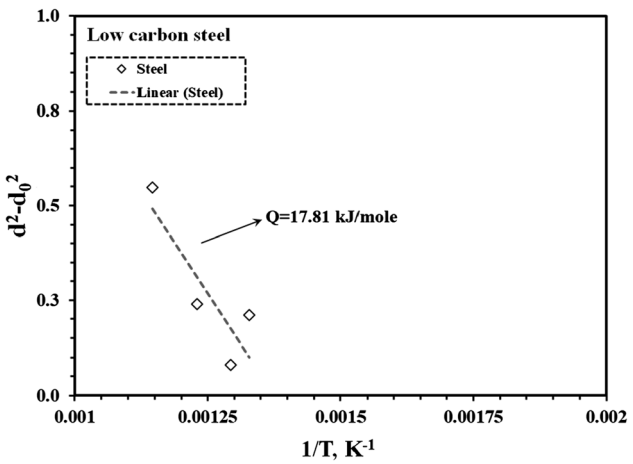

Figure 5 Calculation of activation energy for post-annealing treatment of SPD-modified low-carbon steel.

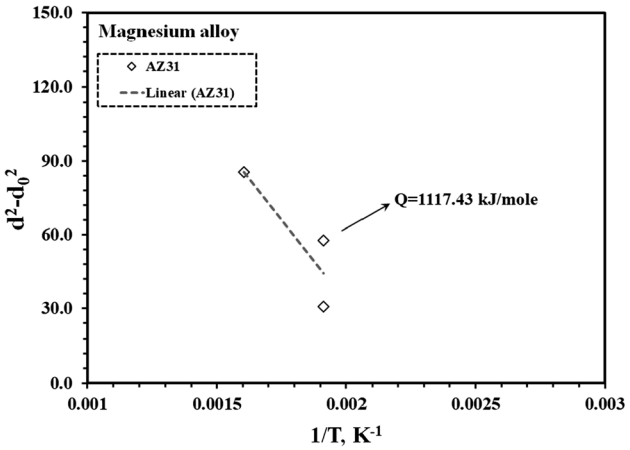

Figure 6 Calculation of activation energy for post-annealing treatment of SPD-modified AZ31 magnesium alloy.

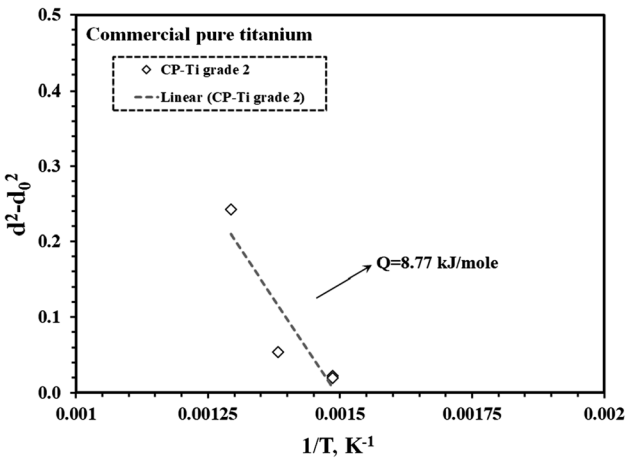

Figure 7 Calculation of activation energy for post-annealing treatment of SPD-modified commercial pure titanium grade 2.

note regarding the calculated activation energies in Figs. 2, 3, 4, 5, 6 and 7, it is noteworthy that the measured values seem all different (almost lower) from the expected values for recrystallization or even self-diffusion of these elements. This is attributed to the other sources for these activation energy calculations, mainly relating to the thermal stability border caused by dislocations annihilation and structural restoration via dynamic recovery and beyond the occurrence of recrystallization. Moreover, the order of activation energy for magnesium alloy is largely varied from the other alloys. That could be due to the micron-scale structural restoration for this alloy by SPD treatment and annealing modification.

Effects of annealing treatment on the direct relationship between SFE level and grain structure of SPD-treated materials

A typical trend observed in this study involves the self-annealing behavior of SPD-modified materials, which is controlled by their thermal stability performance, and this is considerably affected by the melting temperature and SFE value of the examined metals and alloys. By comparing the values listed in Table 7, it seems that for the materials with the same range of melting temperature, reducing the SFE level, the acceleration of the self-annealing process leads to softening which and deteriorated thermal stability [69, 127, 131, 152]. This signifies that a material with a lower SFE value can provide strain hardening for longer times annealing [129, 136]. Although the SFE level is an important parameter to control the annealing-induced softening behavior, having a melting temperature is still a critical factor [130, 137]. Deformation twinning is also a key deformation mechanism which can be accelerated by reducing the SFE level. This twinning mechanism is simultaneously active in conjunction with cross-slip of dislocations to control the microstructural evolution during plastic deformation behavior [153, 154]. In general, annealing of severely deformed materials close to their thermally stable temperature can lead to generation of complex structures with the a combination of recrystallized and non-recrystallized grains as a result of the grain boundary migration, transformation, and rotation mechanisms [33, 69, 140].

By considering a well-accepted dislocation-based model, a general double logarithmic relationship can be established between the smallest achievable grain size and the normalized SFE, as follows [144, 155]:

$$\frac{d_{\min}}{b} = A\left(\frac{\gamma}{Gb}\right)^{q} \tag{6}$$

where $d_{\min}$ is the minimum grain size and b is the Burger's vector. Also, q denotes the exponent for the normalized SFE (~ 0.65), and A presents the dimensionless proportional constant that must be estimated by analyzing the experimental data. Considering this relationship, a finer grain structure can be attained by reducing the SFE value. However, the application of this developed model for alloys rather than the pure materials requires some modification, considering the dependence of dislocation movement and grain structure refinement on the elastic and

modulus mismatches [33, 139]. The double logarithmic illustration of $(\frac{d_{min}}{b})$ versus $(\frac{\gamma}{Gb})$ according to this relation is plotted in Figs. 8 and 9 before and after post-annealing heat treatment, indicating the proportionality constants varied depending on the type of crystallographic structure. As shown for the examined materials with different crystallographic structures of body-centered cubic (BCC), face-centered cubic (FCC), and hexagonal close-packed (HCP), different direct linear correlations between the SFE level and minimum achievable grain size can be established under two differing states of severely deformed and annealed structures. Based on these trends, decreasing the SFE level along with increasing the melting temperature of materials can lead to a considerable reduction in the lowest grain size level upon SPD treatment, mainly by restricting the cross-slip of screw dislocations. In summary, edge or screw dislocation types along with the fraction of cross-slip in the alloy structure and elastic mismatch as well as the modulus interaction between the solute element and metal-matrix are imperative parameters in controlling the dislocations mobility and predicting the structure in severely deformed materials before and after annealing [130, 132, 137].

Summary and concluding remarks

This critical review article assesses the reported information in the literature regarding the stability of ultra-fine and nanoscale grain structures produced by SPD treatment during thermal annealing above

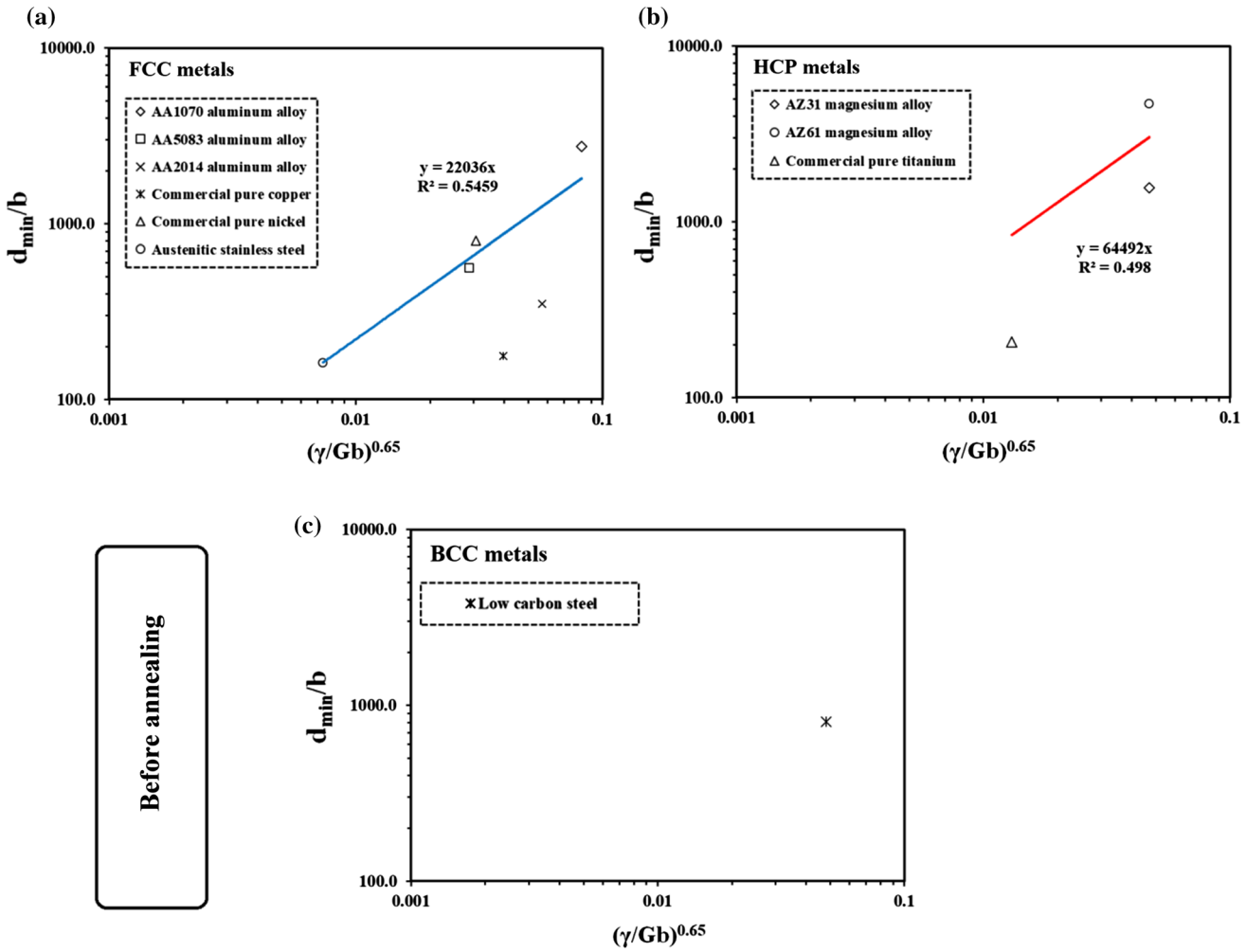

Figure 8 Variation of normalized minimum grain size versus the normalized stacking fault energy according to a logarithmic illustration for the various processed metals and alloys with **a** FCC, **b** HCP, and **c** BCC crystal structures under different SPD treatment routes before post-annealing heat treatment.

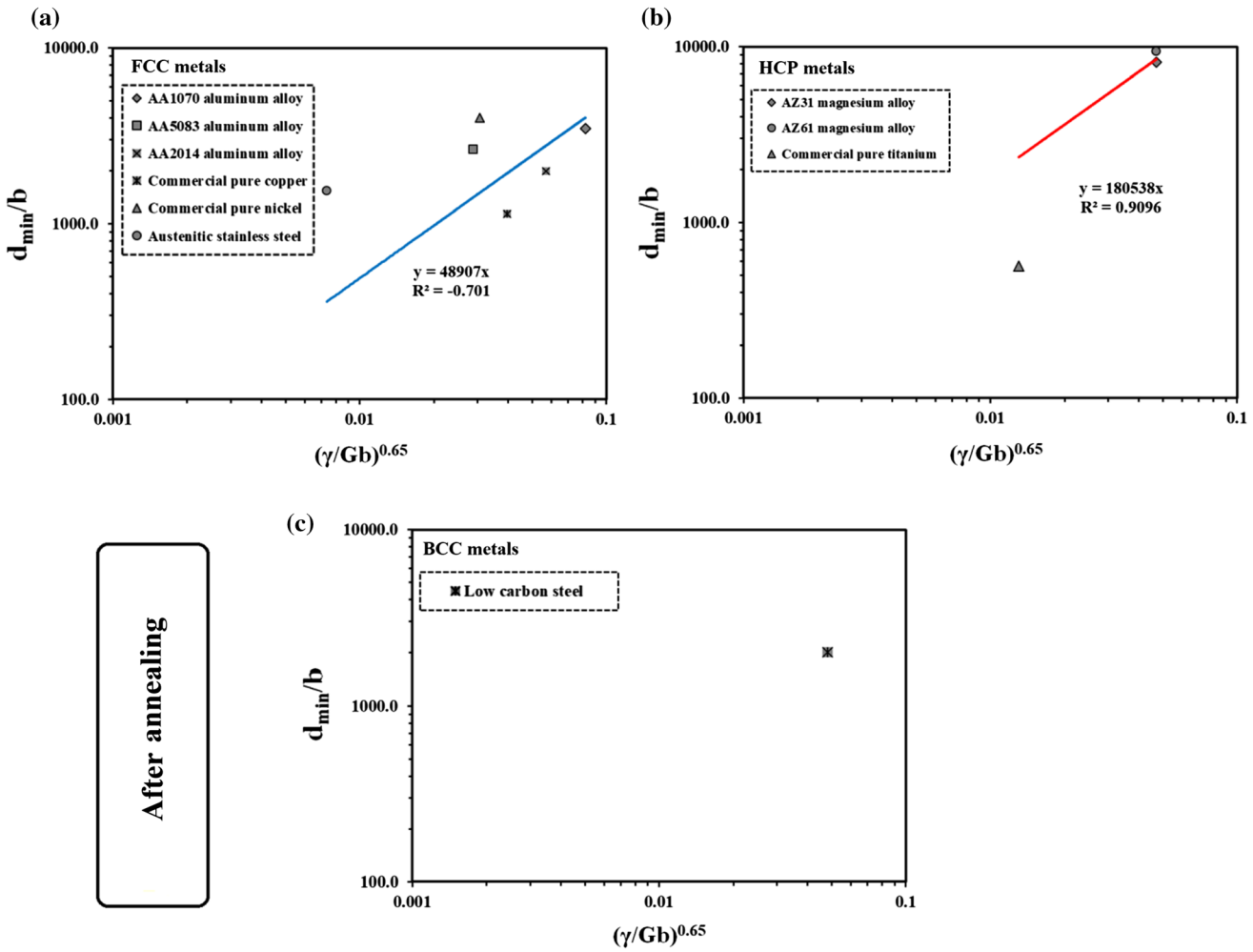

Figure 9 The expressed correlation for the severely deformed materials after post-annealing modification with **a** FCC, **b** HCP, and **c** BCC crystal structures under the optimum range of temperature and time close to the thermal stability condition.

the recrystallization regime. In this context, the results were overviewed and discussed for various metals and alloys (aluminum, copper, nickel, magnesium, steel, and titanium) with different crystal structures (BCC, FCC, and HCP). After SPD modification, the grain structure of materials was refined down to the ranges of 10–400 nm (steel), 45–790 nm (aluminum, copper, nickel), and 60–1500 nm (magnesium and titanium) depending on the type of crystal lattice that can control the number of active slip systems during intense shearing deformation up to high levels of equivalent plastic strains. However, after post-annealing treatment, the static restoration phenomena led to coarsening of strain-induced ultra-fine and nano-grains for the formation of stable microstructures. This structure varies based on by the level of SFE for the examined materials, especially in the case of commercial pure state ones, to control the cross-slip mechanism covering the rearrangement of partial dislocations during dynamic recovery. Accordingly, a linear correlation was established between the SFE state in the range of 10–180 $mJ.m^{-2}$ and stable grain size of severely deformed metals and alloys in the ranges of 40 nm-1.5 μm and 164 nm-3.0 μm upon SPD processing and subsequent post-heating with the different proportionality constants scattered by changing the type of crystal structure as BCC, FCC, and HCP. As a leading concluding issue, by decreasing the SFE, the finer grain structure is achievable during SPD treatment, and the resulting ultra-fine or nano-grains can display a more stable behavior upon thermal annealing due to a higher restriction on the cross-slip phenomenon beyond the occurrence of partial recrystallization.

Perspective and future directions

In the context of enhancing the thermal stability of SPD consolidated UFG/NS metals and alloys to tolerate their subsequent mechanical stability, the interest for future research directions may involve combining the SPD processing routes with the incorporation of reinforcing ceramic nanoparticles to produce ultra-fine grained or nano-structured metal-matrix nano-composites. For these advanced materials, in addition to providing a higher strength-to-weight ratio, since nano-sized particles stabilize the ultra-fine or nanoscale grain boundaries, they can service the required mechanical durability at elevated temperatures by retarding the recrystallization phenomenon. Until now, fascinating results were reported on the thermal stability behavior of SPD-processed metal-matrix nano-composites by ARB, ECAP, HPT, FSP, and AFF routes. However, further developments would be required for future studies.

Declaration

Conflict of interest The authors declare that they have no conflict of interest.

References

[1] Harsha RN, Mithun Kulkarni V, Satish Babu B (2018) Severe plastic deformation a review. Mater. Today 5:22340–22349

[2] Toth LS, Gu C (2014) Ultrafine-grain metals by severe plastic deformation. Mater Charact 92:1–14

[3] Valiev RZ, Islamgaliev RK, Alexandrov IV (2000) Bulk nanostructured materials from severe plastic deformation. Prog Mater Sci 45(2):103–189

[4] Hansen N (2004) Hall-petch relation and boundary strengthening. Scr. Mater. 51(8 SPEC. ISS):801–806

[5] Suryanarayana C, Al-Aqeeli N (2013) Mechanically alloyed nanocomposites. Prog Mater Sci 58(4):383–502

[6] Valiev RZ, Langdon TG (2006) Principles of equal-channel angular pressing as a processing tool for grain refinement. Prog Mater Sci 51(7):881–981

[7] Edalati K, Horita Z (2016) A review on high-pressure torsion (HPT) from 1935 to 1988. Mater. Sci. Eng. A 652:325–352

[8] Kawasaki M, Langdon TG (2014) Review: Achieving superplasticity in metals processed by high-pressure torsion. J Mater Sci 49(19):6487–6496. https://doi.org/10.1007/s10853-014-8204-5

[9] Ghalehbandi SM, Malaki M, Gupta M (2019) Accumulative roll bonding-A review. Appl. Sci. (Switzerland) 9(17):3627

[10] Suryanarayana C (2001) Mechanical alloying and milling. Prog Mater Sci 46(1–2):1–184

[11] Khodabakhshi F, Simchi A (2017) The role of microstructural features on the electrical resistivity and mechanical properties of powder metallurgy Al-SiC-Al_2O_3 nanocomposites. Mater Des 130:26–36

[12] Nosko M, Štepánek M, Zifčák P, Orovčík L, Nagy Š, Dvorák T, Oslanec P, Khodabakhshi F, Gerlich AP (2019) Solid-state joining of powder metallurgy Al-Al_2O_3 nanocomposites via friction-stir welding: Effects of powder particle size on the weldability, microstructure, and mechanical property. Mater. Sci. Eng., A 754:190–204

[13] Mukhtarov S, Dudova N, Valitov V (2009) Processing and mechanical properties of bulk nanostructured nickel-based alloys. Mater. Sci. Eng., A 503(1):181–184

[14] Pachla W, Kulczyk M, Przybysz S, Skiba J, Wojciechowski K, Przybysz M, Topolski K, Sobolewski A, Charkiewicz M (2015) Effect of severe plastic deformation realized by hydrostatic extrusion and rotary swaging on the properties of CP Ti grade 2. J Mater Process Technol 221:255–268

[15] Khodabakhshi F, Kazeminezhad M, Kokabi AH (2010) Constrained groove pressing of low carbon steel: Nanostructure and mechanical properties. Mater. Sci. Eng., A 527(16–17):4043–4049

[16] Shin DH, Park JJ, Kim YS, Park KT (2002) Constrained groove pressing and its application to grain refinement of aluminum. Mater. Sci. Eng., A 328(1–2):98–103

[17] Ma ZY (2008) Friction stir processing technology: a review. Metall Mater Trans A 39(3):642–658

[18] Mishra RS, Ma ZY (2005) Friction stir welding and processing. Mater. Sci. Eng., R 50(1–2):1–78

[19] Khodabakhshi F, Gerlich AP (2018) Accumulative fold-forging (AFF) as a novel severe plastic deformation process to fabricate a high strength ultra-fine grained layered aluminum alloy structure. Mater Charact 136:229–239

[20] Khodabakhshi F, Gerlich AP, Worswick M (2018) Fabrication and characterization of a high strength ultra-fine grained metal-matrix AA8006-B_4C layered nanocomposite by a novel accumulative fold-forging (AFF) process. Mater Des 157:211–226

[21] Segal V (2018) Review: Modes and processes of severe plastic deformation (SPD). Materials 11(7):1175

[22] Figueiredo RB, Langdon TG (2012) Fabricating ultrafine-grained materials through the application of severe plastic deformation: A review of developments in Brazil. J Mater Res Technol 1(1):55–62

[23] Mansoor P, Dasharath SM (2020) Microstructural and mechanical properties of magnesium alloy processed by severe plastic deformation (SPD)-A review. Mater. Today 33:145–154

[24] Faraji G, Kim HS (2017) Review of principles and methods of severe plastic deformation for producing ultrafine-grained tubes. Mater Sci Technol 33(8):905–923

[25] Edalati K (2019) Review on recent advancements in severe plastic deformation of oxides by high-pressure torsion (HPT). Adv Eng Mater 21(1):1800272

[26] Mahmoodian R, Annuar NSM, Faraji G, Bahar ND, Razak BA, Sparham M (2019) Severe Plastic Deformation of Commercial Pure Titanium (CP-Ti) for Biomedical Applications: A Brief Review. JOM 71(1):256–263

[27] Khodabakhshi F, Kazeminezhad M (2011) The annealing phenomena and thermal stability of severely deformed steel sheet. Mater. Sci. Eng., A 528(15):5212–5218

[28] Chinh NQ, Szommer P, Horita Z, Langdon TG (2006) Experimental evidence for grain-boundary sliding in ultra-fine-grained aluminum processed by severe plastic deformation. Adv Mater 18(1):34–39

[29] Etienne A, Radiguet B, Genevois C, Le Breton JM, Valiev R, Pareige P (2010) Thermal stability of ultrafine-grained austenitic stainless steels. Mater. Sci. Eng., A 527(21):5805–5810

[30] Čížek J, Procházka I, Smola B, Stulíková I, Kužel R, Matěj Z, Cherkaska V, Islamgaliev RK, Kulyasova O (2007) Microstructure and thermal stability of ultra fine grained Mg-based alloys prepared by high-pressure torsion. Mater. Sci. Eng., A 462(1):121–126

[31] Emeis F, Peterlechner M, Divinski SV, Wilde G (2018) Grain boundary engineering parameters for ultrafine grained microstructures: Proof of principles by a systematic composition variation in the Cu-Ni system. Acta Mater 150:262–272

[32] Zhilyaev AP, Langdon TG (2008) Using high-pressure torsion for metal processing: Fundamentals and applications. Prog Mater Sci 53(6):893–979

[33] Sakai T, Belyakov A, Kaibyshev R, Miura H, Jonas JJ (2014) Dynamic and post-dynamic recrystallization under hot, cold and severe plastic deformation conditions. Prog Mater Sci 60(1):130–207

[34] Gupta AK, Maddukuri TS, Singh SK (2016) Constrained groove pressing for sheet metal processing. Prog Mater Sci 84:403–462

[35] Heidarzadeh A, Mironov S, Kaibyshev R, Çam G, Simar A, Gerlich A, Khodabakhshi F, Mostafaei A, Field DP, Robson JD, Deschamps A, Withers PJ (2021) Friction stir welding/processing of metals and alloys: A comprehensive review on microstructural evolution. Prog. Mater Sci. 117:100752

[36] Nandan R, DebRoy T, Bhadeshia HKDH (2008) Recent advances in friction-stir welding – Process, weldment structure and properties. Prog Mater Sci 53(6):980–1023

[37] Kawasaki M, Langdon TG (2015) Review: achieving superplastic properties in ultrafine-grained materials at high temperatures. J Mater Sci 51(1):19–32. https://doi.org/10.1007/s10853-015-9176-9

[38] Kumar P, Kawasaki M, Langdon TG (2016) Review: Overcoming the paradox of strength and ductility in ultra-fine-grained materials at low temperatures. J Mater Sci 51(1):7–18. https://doi.org/10.1007/s10853-015-9143-5

[39] Wang Q, Jiang B, Chen D, Jin Z, Zhao L, Yang Q, Huang G, Pan F (2021) Strategies for enhancing the room-temperature stretch formability of magnesium alloy sheets: a review. J Mater Sci 56(23):12965–12998. https://doi.org/10.1007/s10853-021-06067-x

[40] Islamgaliev RK, Yunusova NF, Sabirov IN, Sergueeva AV, Valiev RZ (2001) Deformation behavior of nanostructured aluminum alloy processed by severe plastic deformation. Mater. Sci. Eng., A 319–321:877–881

[41] Krishnaiah A, Chakkingal U, Venugopal P (2005) Production of ultrafine grain sizes in aluminium sheets by severe plastic deformation using the technique of groove pressing. Scr Mater 52(12):1229–1233

[42] Senkov ON, Froes FH, Stolyarov VV, Valiev RZ, Liu J (1998) Microstructure of aluminum-iron alloys subjected to severe plastic deformation. Scr Mater 38(10):1511–1516

[43] Yin J, Lu J, Ma H, Zhang P (2004) Nanostructural formation of fine grained aluminum alloy by severe plastic deformation at cryogenic temperature. J Mater Sci 39(8):2851–2854. https://doi.org/10.1023/B:JMSC.0000021463.83899.b3

[44] Sabirov I, Murashkin MY, Valiev RZ (2013) Nanostructured aluminium alloys produced by severe plastic deformation: New horizons in development. Mater. Sci. Eng., A 560:1–24

[45] Abdulstaar MA, El-Danaf EA, Waluyo NS, Wagner L (2013) Severe plastic deformation of commercial purity aluminum by rotary swaging: Microstructure evolution and mechanical properties. Mater. Sci. Eng., A 565:351–358

[46] Leo P, Cerri E, De Marco PP, Roven HJ (2007) Properties and deformation behaviour of severe plastic deformed aluminium alloys. J Mater Process Technol 182(1–3):207–214

[47] Markushev MV, Bampton CC, Murashkin MY, Hardwick DA (1997) Structure and properties of ultra-fine grained aluminium alloys produced by severe plastic deformation. Mater. Sci. Eng., A 234–236:927–931

[48] May J, Höppel HW, Göken M (2005) Strain rate sensitivity of ultrafine-grained aluminium processed by severe plastic deformation. Scr Mater 53(2):189–194

[49] Roven HJ, Liu M, Werenskiold JC (2008) Dynamic precipitation during severe plastic deformation of an Al-Mg-Si aluminium alloy. Mater. Sci. Eng., A 483–484(1–2C):54–58

[50] Biswas S, Singh Dhinwal S, Suwas S (2010) Room-temperature equal channel angular extrusion of pure magnesium. Acta Mater. 58(9):3247–3261

[51] Lee S, Berbon PB, Furukawa M, Horita Z, Nemoto M, Tsenev NK, Valiev RZ, Langdon TG (1999) Developing superplastic properties in an aluminum alloy through severe plastic deformation. Mater. Sci. Eng., A 272(1):63–72

[52] Dhal A, Panigrahi SK, Shunmugam MS (2017) Insight into the microstructural evolution during cryo-severe plastic deformation and post-deformation annealing of aluminum and its alloys. J Alloys Compd 726:1205–1219

[53] Divinski SV, Padmanabhan KA, Wilde G (2011) Microstructure evolution during severe plastic deformation. Philos Mag 91(36):4574–4593

[54] Estrin Y, Vinogradov A (2010) Fatigue behaviour of light alloys with ultrafine grain structure produced by severe plastic deformation: An overview. Int J Fatigue 32(6):898–907

[55] Estrin Y, Vinogradov A (2013) Extreme grain refinement by severe plastic deformation: A wealth of challenging science. Acta Mater 61(3):782–817

[56] Khodabakhshi F, Gerlich AP, Simchi A, Kokabi AH (2015) Cryogenic friction-stir processing of ultrafine-grained Al–Mg–TiO_2 nanocomposites. Mater. Sci. Eng., A 620:471–482

[57] Gubicza J, El-Tahawy M, Lábár JL, Bobruk EV, Murashkin MY, Valiev RZ, Chinh NQ (2020) Evolution of microstructure and hardness during artificial aging of an ultrafine-grained Al-Zn-Mg-Zr alloy processed by high pressure torsion. J Mater Sci 55(35):16791–16805. https://doi.org/10.1007/s10853-020-05264-4

[58] Horita Z, Fujinami T, Nemoto M, Langdon TG (2001) Improvement of mechanical properties for Al alloys using equal-channel angular pressing. J Mater Process Technol 117(3):288–292

[59] Sauvage X, Wilde G, Divinski SV, Horita Z, Valiev RZ (2012) Grain boundaries in ultrafine grained materials processed by severe plastic deformation and related phenomena. Mater. Sci. Eng., A 540:1–12

[60] Zhu YT, Liao XZ, Srinivasan SG, Lavernia EJ (2005) Nucleation of deformation twins in nanocrystalline face-centered-cubic metals processed by severe plastic deformation. J. Appl. Phys. 98(3):034319

[61] Ivanov KV, Ovcharenko VE (2020) Structural features of ultrafine-grained aluminum processed through accumulative roll bonding providing improved mechanical properties and thermal stability. Mater. Sci. Eng., A 775:138988

[62] Mazilkin AA, Myshlyaev MM (2006) Microstructure and thermal stability of superplastic aluminium-lithium alloy after severe plastic deformation. J Mater Sci 41(12):3767–3772. https://doi.org/10.1007/s10853-006-2637-4

[63] Mao J, Kang SB, Park JO (2005) Grain refinement, thermal stability and tensile properties of 2024 aluminum alloy after equal-channel angular pressing. J Mater Process Technol 159(3):314–320

[64] Adamczyk-Cieślak B, Mizera J, Kurzydłowski KJ (2010) Thermal stability of model Al–Li alloys after severe plastic deformation—Effect of the solute Li atoms. Mater. Sci. Eng., A 527(18):4716–4722

[65] McKenzie PWJ, Lapovok R (2010) ECAP with back pressure for optimum strength and ductility in aluminium alloy 6016. Part 1: Microstructure. Acta Mater. 58(9):3198–3211

[66] Mohamed IF, Yonenaga Y, Lee S, Edalati K, Horita Z (2015) Age hardening and thermal stability of Al–Cu alloy processed by high-pressure torsion. Mater. Sci. Eng., A 627:111–118

[67] Saldana C, King AH, Chandrasekar S (2012) Thermal stability and strength of deformation microstructures in pure copper. Acta Mater 60(10):4107–4116

[68] Edalati K, Hashiguchi Y, Iwaoka H, Matsunaga H, Valiev RZ, Horita Z (2018) Long-time stability of metals after severe plastic deformation: Softening and hardening by self-annealing versus thermal stability. Mater. Sci. Eng., A 729:340–348

[69] Zhao YH, Liao XZ, Zhu YT, Horita Z, Langdon TG (2005) Influence of stacking fault energy on nanostructure formation under high pressure torsion. Mater. Sci. Eng., A 410–411:188–193

[70] Yu H, Wang L, Chai L, Li J, Lu C, Godbole A, Wang H, Kong C (2019) High thermal stability and excellent mechanical properties of ultrafine-grained high-purity copper sheets subjected to asymmetric cryorolling. Mater Charact 153:34–45

[71] Fernandez-Zelaia P, Melkote SN (2019) Process–structure–property relationships in bimodal machined microstructures using robust structure descriptors. J. Mater. Process. Technol. 273:116251

[72] Rodríguez-Calvillo P, Ferrer N, Cabrera JM (2015) Analysis of microstructure and strengthening in CuMg alloys deformed by equal channel angular pressing. J Alloys Compd 626:340–348

[73] Azzeddine H, Bourezg YI, Khereddine AY, Baudin T, Helbert AL, Brisset F, Kawasaki M, Bradai D, Langdon TG (2020) An investigation of the stored energy and thermal stability in a Cu–Ni–Si alloy processed by high-pressure torsion. Philos Mag 100(6):688–712

[74] Primorac MM, Abad MD, Hosemann P, Kreuzeder M, Maier V, Kiener D (2015) Elevated temperature mechanical properties of novel ultra-fine grained Cu–Nb composites. Mater. Sci. Eng., A 625:296–302

[75] Wilde G, Rösner H (2007) Stability aspects of bulk nanostructured metals and composites. J Mater Sci 42(5):1772–1781. https://doi.org/10.1007/s10853-006-0986-7

[76] Islamgaliev RK, Chmelik F, Kuzel R (1997) Thermal structure changes in copper and nickel processed by severe plastic deformation. Mater. Sci. Eng., A 234–236:335–338

[77] Ibrahim N, Peterlechner M, Emeis F, Wegner M, Divinski SV, Wilde G (2017) Mechanical alloying via high-pressure torsion of the immiscible Cu50Ta50 system. Mater. Sci. Eng., A 685:19–30

[78] Islamgaliev RK, Buchgraber W, Kolobov YR, Amirkhanov NM, Sergueeva AV, Ivanov KV, Grabovetskaya GP (2001) Deformation behavior of Cu-based nanocomposite processed by severe plastic deformation. Mater. Sci. Eng., A 319–321:872–876

[79] Vinogradov A, Patlan V, Suzuki Y, Kitagawa K, Kopylov VI (2002) Structure and properties of ultra-fine grain Cu–Cr–Zr alloy produced by equal-channel angular pressing. Acta Mater 50(7):1639–1651

[80] Bachmaier A, Pfaff M, Stolpe M, Aboulfadl H, Motz C (2015) Phase separation of a supersaturated nanocrystalline Cu–Co alloy and its influence on thermal stability. Acta Mater 96:269–283

[81] Qi Y, Kosinova A, Kilmametov AR, Straumal BB, Rabkin E (2020) Stabilization of ultrafine-grained microstructure in high-purity copper by gas-filled pores produced by severe plastic deformation. Scr Mater 178:29–33

[82] Islamgaliev RK, Chmelik F, Kuzel R (1997) Thermal stability of submicron grained copper and nickel. Mater. Sci. Eng., A 237(1):43–51

[83] Gubicza J, Nam NH, Balogh L, Hellmig RJ, Stolyarov VV, Estrin Y, Ungár T (2004) Microstructure of severely deformed metals determined by X-ray peak profile analysis. J Alloys Compd 378(1):248–252

[84] Lugo N, Llorca N, Suñol JJ, Cabrera JM (2010) Thermal stability of ultrafine grains size of pure copper obtained by equal-channel angular pressing. J Mater Sci 45(9):2264–2273

[85] Jayakumar PK, Balasubramanian K, Rabindranath Tagore G (2012) Recrystallisation and bonding behaviour of ultra fine grained copper and Cu–Cr–Zr alloy using ECAP. Mater. Sci. Eng., A 538:7–13

[86] Lomakin I, Castillo-Rodríguez M, Sauvage X (2019) Microstructure, mechanical properties and aging behaviour of nanocrystalline copper–beryllium alloy. Mater. Sci. Eng., A 744:206–214

[87] Yadav PC, Sharma NK, Sahu S, Shekhar S (2019) Influence of short heat-treatment on microstructural and mechanical inhomogeneity of constrained groove pressed Cu-Zn alloy. Mater. Chem. Phys. 238:121912

[88] Zhilyaev AP, Nurislamova GV, Valiev RZ, Baro MD, Langdon TG (2002) Thermal stability and microstructural evolution in ultrafine-grained nickel after equal-channel angular pressing (ECAP). Metall Mater Trans A 33(6):1865–1868

[89] Korznikov AV, Dimitrov O, Korznikova GF, Dallas JP, Idrisova SR, Valiev RZ, Faudot F (1999) Thermal evolution of high-purity and boron-doped sub-microcrystalline Ni_3Al produced by severe plastic deformation. Acta Mater 47(11):3301–3311

[90] Ravi Shankar M, Rao BC, Chandrasekar S, Dale Compton W, King AH (2008) Thermally stable nanostructured materials from severe plastic deformation of precipitation-treatable Ni-based alloys. Scr. Mater. 58(8):675–678

[91] Aristizabal K, Katzensteiner A, Bachmaier A, Mücklich F, Suárez S (2020) Microstructural evolution during heating of CNT/Metal Matrix Composites processed by Severe Plastic Deformation. Sci Rep 10(1):857

[92] Bachmaier A, Katzensteiner A, Wurster S, Aristizabal K, Suarez S, Pippan R (2020) Thermal stabilization of metal matrix nanocomposites by nanocarbon reinforcements. Scr Mater 186:202–207

[93] Popov VV, Popova EN, Kuznetsov DD, Stolbovsky AV, Shorohov EV, Nasonov PA, Gaan KA, Reglitz G, Divinski SV, Wilde G (2013) Evolution of Ni structure at dynamic channel-angular pressing. Mater. Sci. Eng., A 585:281–291

[94] Wang Z, Guan Y, Li L, Zhu L (2019) The fracture behavior and thermal stability of commercially pure nickel sheets processed by constrained groove pressing. Metals 9(10):1047

[95] Sauvage X, Ivanisenko Y (2007) The role of carbon segregation on nanocrystallisation of pearlitic steels processed by severe plastic deformation. J Mater Sci 42(5):1615–1621. https://doi.org/10.1007/s10853-006-0750-z

[96] Wetscher F, Vorhauer A, Stock R, Pippan R (2004) Structural refinement of low alloyed steels during severe plastic deformation. Mater. Sci. Eng., A 387–389(1–2 SPEC. ISS.):809–816

[97] Korznikov AV, Ivanisenko YV, Laptionok DV, Safarov IM, Pilyugin VP, Valiev RZ (1994) Influence of severe plastic deformation on structure and phase composition of carbon steel. Nanostruct Mater 4(2):159–167

[98] Umemoto M (2003) Nanocrystallization of Steels by Severe Plastic Deformation. Mater Trans 44(10):1900–1911

[99] Shin DH, Park JJ, Chang SY, Lee YK, Park KT (2002) Ultrafine Grained Low Carbon Steels Fabricated by Equal Channel Angular Pressing: Microstructures and Tensile Properties. ISIJ Int 42(12):1490–1496

[100] Ivanisenko YV, Korznikov AV, Safarov IM, Valiev RZ (1995) Formation of submicrocrystalline structure in iron and its alloys after severe plastic deformation. Nanostruct Mater 6(1):433–436

[101] Khodabakhshi F, Kazeminezhad M (2014) Differential scanning calorimetry study of constrained groove pressed low carbon steel: Recovery, recrystallisation and ferrite to austenite phase transformation. Mater Sci Technol 30(7):765–773

[102] Ivanisenko Y, Wunderlich RK, Valiev RZ, Fecht HJ (2003) Annealing behaviour of nanostructured carbon steel produced by severe plastic deformation. Scr. Mater. 49(10 SPEC.):947–952

[103] Park KT, Kim YS, Lee JG, Shin DH (2000) Thermal stability and mechanical properties of ultrafine grained low carbon steel. Mater. Sci. Eng., A 293(1):165–172

[104] Duan J, Wen H, Zhou C, He X, Islamgaliev R, Valiev R (2020) Annealing behavior in a high-pressure torsion-processed Fe–9Cr steel. J Mater Sci 55(18):7958–7968

[105] Hao T, Fan ZQ, Zhao SX, Luo GN, Liu CS, Fang QF (2014) Strengthening mechanism and thermal stability of severely deformed ferritic/martensitic steel. Mater. Sci. Eng., A 596:244–249

[106] Khodabakhshi F, Kazeminezhad M (2011) The effect of constrained groove pressing on grain size, dislocation density and electrical resistivity of low carbon steel. Mater Des 32(6):3280–3286

[107] Ivanisenko Y, Wunderlich RK, Valiev RZ, Fecht HJ (2003) Annealing behaviour of nanostructured carbon steel produced by severe plastic deformation. Scr Mater 49(10):947–952

[108] Figueiredo RB, Langdon TG (2009) Strategies for achieving high strain rate superplasticity in magnesium alloys processed by equal-channel angular pressing. Scr Mater 61(1):84–87

[109] Kim WJ, Lee BH, Lee JB, Lee MJ, Park YB (2010) Synthesis of high-strain-rate superplastic magnesium alloy sheets using a high-ratio differential speed rolling technique. Scr Mater 63(7):772–775

[110] Hamu GB, Eliezer D, Wagner L (2009) The relation between severe plastic deformation microstructure and corrosion behavior of AZ31 magnesium alloy. J Alloys Compd 468(1–2):222–229

[111] Yamashita A, Horita Z, Langdon TG (2001) Improving the mechanical properties of magnesium and a magnesium alloy through severe plastic deformation. Mater. Sci. Eng., A 300(1–2):142–147

[112] Kim WJ, Park IB (2013) Enhanced superplasticity and diffusional creep in ultrafine-grained Mg–6Al–1Zn alloy with high thermal stability. Scr Mater 68(3):179–182

[113] Edalati K, Kitabayashi K, Ikeda Y, Matsuda J, Li HW, Tanaka I, Akiba E, Horita Z (2018) Bulk nanocrystalline gamma magnesium hydride with low dehydrogenation temperature stabilized by plastic straining via high-pressure torsion. Scr Mater 157:54–57

[114] Lee TJ, Kim WJ (2020) Successful transition from low-temperature superplasticity to high-strain-rate superplasticity with increasing temperature in an ultrafine-grained Mg–Y–Zn–Zr alloy. J. Alloys Compd. 817:153298

[115] Jamalian M, Reeve JI, Field DP (2020) Thermal behavior of AZ31 gradient microstructure after cold severe surface plastic deformation. Mater. Charact. 169:110630

[116] Fong KS, Danno A, Tan MJ, Chua BW (2017) Tensile flow behavior of AZ31 magnesium alloy processed by severe plastic deformation and post-annealing at moderately high temperatures. J Mater Process Technol 246:235–244

[117] Eddahbi M, Valle JAD, Pérez-Prado MT, Ruano OA (2005) Comparison of the microstructure and thermal stability of an AZ31 alloy processed by ECAP and large strain hot rolling. Mater. Sci. Eng., A 410–411:308–311

[118] Choi HY, Kim WJ (2015) Effect of thermal treatment on the bio-corrosion and mechanical properties of ultrafine-grained ZK60 magnesium alloy. J Mech Behav Biomed Mater 51:291–301

[119] del Valle JA, Peñalba F, Ruano OA (2007) Optimization of the microstructure for improving superplastic forming in magnesium alloys. Mater. Sci. Eng., A 467(1):165–171

[120] Stráská J, Janeček M, Čížek J, Stráský J, Hadzima B (2014) Microstructure stability of ultra-fine grained magnesium alloy AZ31 processed by extrusion and equal-channel angular pressing (EX–ECAP). Mater Charact 94:69–79

[121] Young JP, Askari H, Hovanski Y, Heiden MJ, Field DP (2015) Thermal microstructural stability of AZ31 magnesium after severe plastic deformation. Mater Charact 101:9–19

[122] Tang L, Zhao Y, Islamgaliev RK, Valiev RZ, Zhu YT (2017) Microstructure and thermal stability of nanocrystalline Mg-Gd-Y-Zr alloy processed by high pressure torsion. J Alloys Compd 721:577–585

[123] Stolyarov VV, Zhu YT, Alexandrov IV, Lowe TC, Valiev RZ (2003) Grain refinement and properties of pure Ti processed by warm ECAP and cold rolling. Mater. Sci. Eng., A 343(1):43–50

[124] Völker B, Maier-Kiener V, Werbach K, Müller T, Pilz S, Calin M, Eckert J, Hohenwarter A (2019) Influence of annealing on microstructure and mechanical properties of ultrafine-grained Ti45Nb. Mater. Des. 179:107864

[125] Stolyarov VV, Zeipper L, Mingler B, Zehetbauer M (2008) Influence of post-deformation on CP-Ti processed by equal channel angular pressing. Mater. Sci. Eng., A 476(1):98–105

[126] Li Z, Fu L, Fu B, Shan A (2012) Effects of annealing on microstructure and mechanical properties of nano-grained titanium produced by combination of asymmetric and symmetric rolling. Mater. Sci. Eng., A 558:309–318

[127] Zhao YH, Zhu YT, Liao XZ, Horita Z, Langdon TG (2007) Influence of stacking fault energy on the minimum grain size achieved in severe plastic deformation. Mater. Sci. Eng., A 463(1–2):22–26

[128] Zhao YH, Liao XZ, Horita Z, Langdon TG, Zhu YT (2008) Determining the optimal stacking fault energy for achieving high ductility in ultrafine-grained Cu-Zn alloys. Mater. Sci. Eng., A 493(1–2):123–129

[129] Zhao YH, Zhu YT, Liao XZ, Horita Z, Langdon TG (2006) Tailoring stacking fault energy for high ductility and high strength in ultrafine grained Cu and its alloy. Appl. Phys. Lett. 89(12):121906

[130] Edalati K, Akama D, Nishio A, Lee S, Yonenaga Y, Cubero-Sesin JM, Horita Z (2014) Influence of dislocation-solute atom interactions and stacking fault energy on grain size of single-phase alloys after severe plastic deformation using high-pressure torsion. Acta Mater 69:68–77

[131] Edalati K, Horita Z (2011) Significance of homologous temperature in softening behavior and grain size of pure metals processed by high-pressure torsion. Mater. Sci. Eng., A 528(25–26):7514–7523

[132] Edalati K, Horita Z (2011) High-pressure torsion of pure metals: Influence of atomic bond parameters and stacking fault energy on grain size and correlation with hardness. Acta Mater 59(17):6831–6836

[133] Setman D, Schafler E, Korznikova E, Zehetbauer MJ (2008) The presence and nature of vacancy type defects in nanometals detained by severe plastic deformation. Mater. Sci. Eng., A 493(1–2):116–122

[134] Balogh L, Ungár T, Zhao Y, Zhu YT, Horita Z, Xu C, Langdon TG (2008) Influence of stacking-fault energy on microstructural characteristics of ultrafine-grain copper and copper-zinc alloys. Acta Mater 56(4):809–820

[135] Zhao YH, Horita Z, Langdon TG, Zhu YT (2008) Evolution of defect structures during cold rolling of ultrafine-grained Cu and Cu-Zn alloys: Influence of stacking fault energy. Mater. Sci. Eng., A 474(1–2):342–347

[136] Sarma VS, Wang J, Jian WW, Kauffmann A, Conrad H, Freudenberger J, Zhu YT (2010) Role of stacking fault energy in strengthening due to cryo-deformation of FCC metals. Mater. Sci. Eng. A 527(29–30):7624–7630

[137] Misra RDK, Challa VSA, Venkatsurya PKC, Shen YF, Somani MC, Karjalainen LP (2015) Interplay between grain structure, deformation mechanisms and austenite stability in phase-reversion-induced nanograined/ultrafine-grained austenitic ferrous alloy. Acta Mater 84:339–348

[138] Reed-Hill RE, Abbaschian R (1973) Physical metallurgy principles, Van Nostrand.

[139] Alaneme KK, Okotete EA (2017) Enhancing plastic deformability of Mg and its alloys—A review of traditional and nascent developments. J Magnes Alloy 5(4):460–475

[140] Villegas JC, Shaw LL (2009) Nanocrystallization process and mechanism in a nickel alloy subjected to surface severe plastic deformation. Acta Mater 57(19):5782–5795

[141] Khodabakhshi F, Gerlich AP, Simchi A, Kokabi AH (2015) Hot deformation behavior of an aluminum-matrix hybrid nanocomposite fabricated by friction stir processing. Mater. Sci. Eng., A 626:458–466

[142] Khodabakhshi F, Gerlich AP, Verma D, Nosko M, Haghshenas M (2021) Depth-sensing thermal stability of accumulative fold-forged nanostructured materials. Mater. Des. 202:109554

[143] Murr LE (1973) Twin boundary energetics in pure aluminium. Acta Metall 21(6):791–797

[144] Morishige T, Hirata T, Uesugi T, Takigawa Y, Tsujikawa M, Higashi K (2011) Effect of Mg content on the minimum grain size of Al–Mg alloys obtained by friction stir processing. Scr Mater 64(4):355–358

[145] Hertzberg RW, Vinci RP, Hertzberg JL (2013) Deformation and fracture mechanics of engineering materials. Wiley, New York, p 80

[146] Gallagher PCJ (1970) The influence of alloying, temperature, and related effects on the stacking fault energy. Metall Trans 1(9):2429–2461

[147] Edalati K, Akama D, Nishio A, Lee S, Yonenaga Y, Cubero-Sesin JM, Horita Z (2014) Influence of dislocation–solute atom interactions and stacking fault energy on grain size of single-phase alloys after severe plastic deformation using high-pressure torsion. Acta Mater 69:68–77

[148] Heidarzadeh A, Saeid T, Klemm V, Chabok A, Pei Y (2019) Effect of stacking fault energy on the restoration mechanisms and mechanical properties of friction stir welded copper alloys. Mater Des 162:185–197

[149] Feng Z, Zhang X, Pan F (2012) Influence of solute and solute segregation on the stacking fault energy in hcp metals. Xiyou Jinshu Cailiao Yu Gongcheng/Rare Metal Materials and Engineering 41(10):1765–1769

[150] Guo Z, Miodownik AP, Saunders N, Schillé JP (2006) Influence of stacking-fault energy on high temperature creep of alpha titanium alloys. Scr Mater 54(12):2175–2178

[151] Dhal A, Panigrahi SK, Shunmugam MS, Precipitation phenomena, thermal stability and grain growth kinetics in an ultra-fine grained Al, (2014) alloy after annealing treatment. J Alloys Compd 649(2015):229–238

[152] Edalati K, Fujioka T, Horita Z (2008) Microstructure and mechanical properties of pure Cu processed by high-pressure torsion. Mater. Sci. Eng., A 497(1–2):168–173

[153] Gubicza J, Chinh NQ, Lábár JL, Hegedűs Z, Langdon TG (2009) Twinning and dislocation activity in silver processed by severe plastic deformation. J Mater Sci 44(6):1656–1660. https://doi.org/10.1007/s10853-009-3278-1

[154] Karaman I, Yapici GG, Chumlyakov YI, Kireeva IV (2005) Deformation twinning in difficult-to-work alloys during severe plastic deformation. Mater. Sci. Eng., A 410–411:243–247

[155] Mohamed FA (2003) A dislocation model for the minimum grain size obtainable by milling. Acta Mater 51(14):4107–4119